Silica-Supported Isolated Gallium Sites as Highly Active, Selective and Stable Propane Dehydrogenation Catalysts

Keith Searles, Georges Siddiqi, Olga V. Safonova, Christophe Copéret.*

Supporting Information

Experimental Details

General procedures: Unless otherwise stated, all operations were performed in a M. Braun Lab Master dry box under an argon atmosphere or using high vacuum standard Schlenk techniques under an argon atmosphere. Pentane was sparged with argon for 30 minutes and dried using a two-column solvent purification system where columns designated for pentane were packed with activated alumina. Tetrahydrofuran was distilled from purple Na^0/benzophenone under argon. Benzene and deuterated benzene (C_6D_6) were vacuum distilled from purple Na^0/benzophenone. All solvents were stored over 4 Å molecular sieves after being transferred to a glove box. Celite and 4 Å molecular sieves were activated under high vacuum overnight at 300 ºC. $SiO_{2\text{-}700}$ was prepared by heating Degauss Aerosil (204 m^2/g) to 500 ºC (5 ºC/min), calcining in air for 4 hours, evacuating to high vacuum (10^{-5} mbar), maintaining a temperature of 500 ºC for 8 hours, heating to 700 ºC (5 ºC/min), and maintaining 700 ºC for 12 hours. Titration of the $SiO_{2\text{-}700}$ using $[Mg(CH_2Ph)_2(THF)_2]$ yielded 0.31 mmol OH g^{-1} corresponding to 0.92 accessible OH groups per nm^2. $NaOSi(O\textit{t}Bu)_3$ was prepared according to literature procedures.[1] $[Ga(OSi(O\textit{t}Bu)_3)_3(THF)]$ was prepared using modification of a recent literature report.[2] All other reagents were purchased from Sigma-Aldrich or Strem Chemicals and used as received. Transmission infrared spectra were recorded using a Bruker Alpha FT-IR spectrometer. Solution ^1H and ^{13}C NMR spectra were recorded on a Bruker 300 MHz NMR spectrometer. Solution ^1H and $^{13}C\{^1H\}$ NMR spectra are reported with reference to residual ^1H solvent resonances of C_6D_6 at 7.16 and 128.06 ppm, respectively. Solid-state NMR spectra were recorded on a Bruker 400 MHz NMR spectrometer using a triple resonance 4 mm CP-MAS probe. Samples were packed in 4 mm zirconia rotors and referenced to adamantine at 38.44 ppm. Mikroanalytisches Labor Pascher located in Remagen, Germany performed elemental analyses.

Synthesis of [Ga(OSi(O*t*Bu)$_3$)$_3$(THF)] (1). To a 20 mL THF solution of $GaCl_3$ (0.342 g, 1.94 mmol) cooled to 0 °C was added drop wise a 100 mL THF solution of $NaOSi(O\textit{t}Bu)_3$ (1.670 g, 5.83 mmol) cooled to 0 °C. Upon addition of the $GaCl_3$ solution a white precipitate formed. The solution was stirred for 12 hours while slowly warming to room temperature. The volatiles were subsequently removed from the reaction mixture under reduced pressure. To the resulting white solid was added 30 mL of pentane and the reaction mixture was filtered through a celite plug supported on a glass frit. The colorless filtrate was concentrated to ca. 10 mL and stored at -40 °C resulting in formation of colorless crystals. The crystals were isolated on a glass frit and dried under reduced pressure yielding 1.552 g of pure material. Single crystals suitable for X-ray diffraction analysis were obtained from a concentrated pentane solution stored at -40 °C for 4 days. Yield = 86.1 % (1.552 g, 1.67 mmol). **^{1}H NMR (25 °C, 300 MHz, C_6D_6):** δ 4.44 (s, 4H, -C*H*$_2$-$_{THF}$), 1.52 (m, 85 H, -C(C*H*$_3$)$_3$ and -C*H*$_2$-$_{THF}$). **^{13}C{^{1}H} NMR (25 °C, 75 MHz, C_6D_6):** 71.97 (s, -*C*(CH$_3$)$_3$), 32.18 (s, -C(*C*H$_3$)$_3$), 25.06 (s, -*C*H$_2$-$_{THF}$).

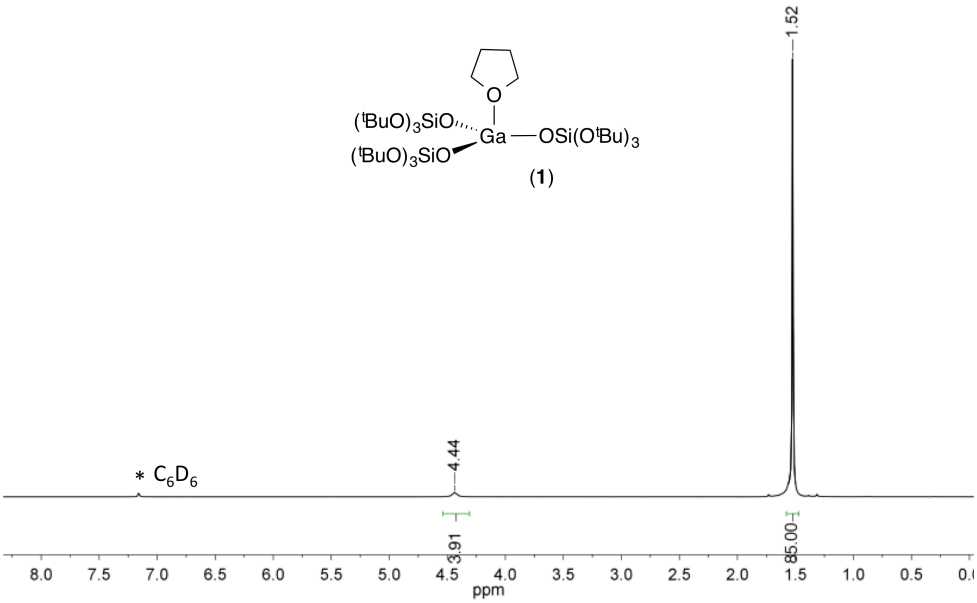

Figure S1. ^{1}H NMR spectrum of **1** recorded in C_6D_6 (300 MHz, 25°C).

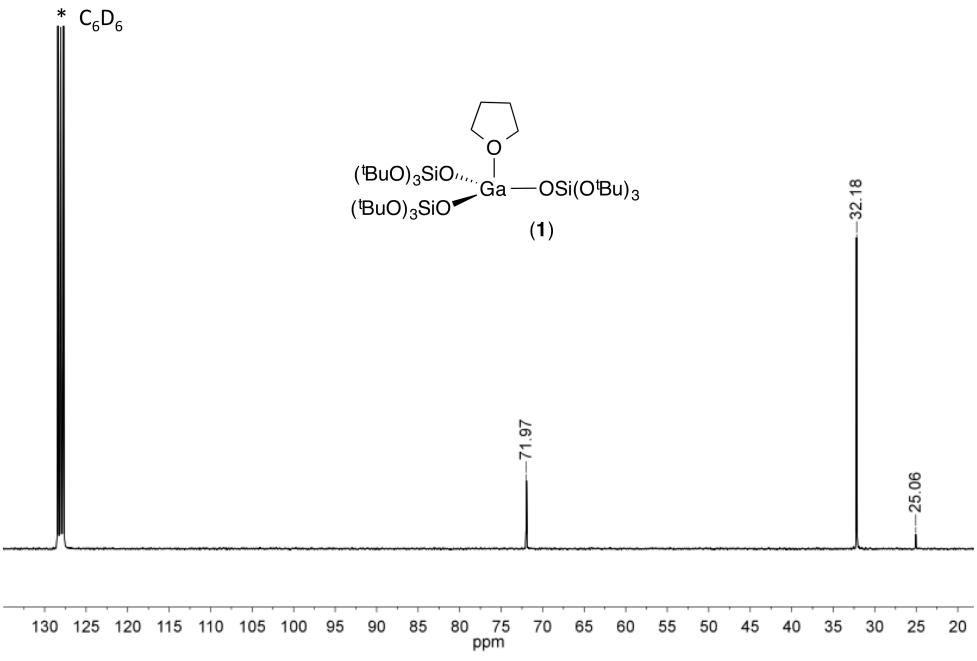

Figure S2. ^{13}C NMR spectrum of **1** recorded in C_6D_6 (75 MHz, 25°C).

Synthesis of [(≡SiO)$_3$Ga(HOR)], (R = –Si(O*t*Bu)$_3$ or –*t*Bu) (2).

To a suspension of $SiO_{2\text{-}700}$ (2.007 g, 0.622 mmol –OH) in C_6H_6 was added a clear solution of **1** (0.571 g, 0.613 mmol). The suspension was stirred for 12 hours at 25 °C. After stirring the material was filtered, washed with C_6H_6 (4 x 5 mL) and dried under under high vacuum (10^{-5} mbar). Using ^{1}H NMR spectroscopy (300 MHz, 25 °C, d1 = 60 sec) with ferrocene as an internal standard, isobutene (4.3 eq), *tert*-butanol (1.9 eq), and THF (1.0 eq) were quantified as side products of the reaction. Elemental analysis: Ga, 1.53; C, 2.40; H, 0.50.

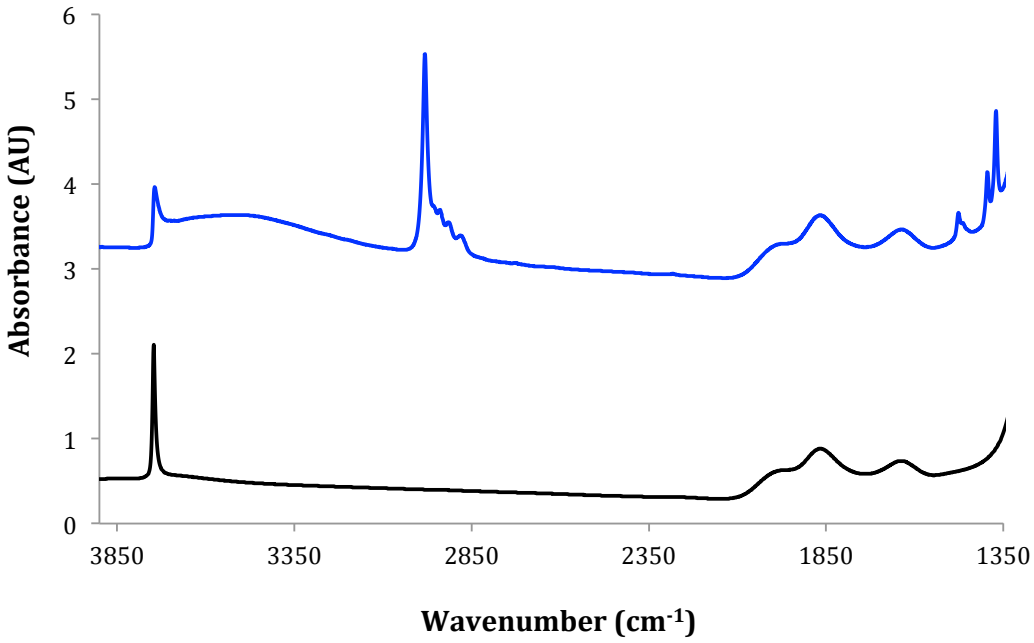

Figure S3. Transmission IR spectra of **2** (top) and $SiO_{2\text{-}700}$ (bottom) normalized to the υ_{SiO} vibrational band at 1850 cm^{-1}.

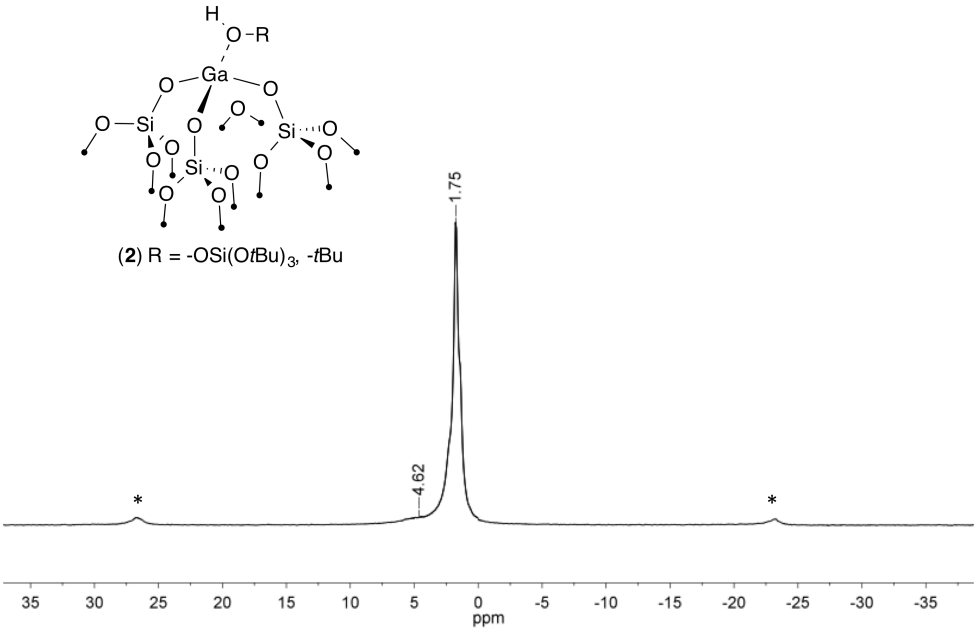

Figure S4. ^{1}H SSNMR of **2** (spinning rate, 10 kHz; scans, 8; line broadening, 8 Hz). Spinning side bands are denoted with *.

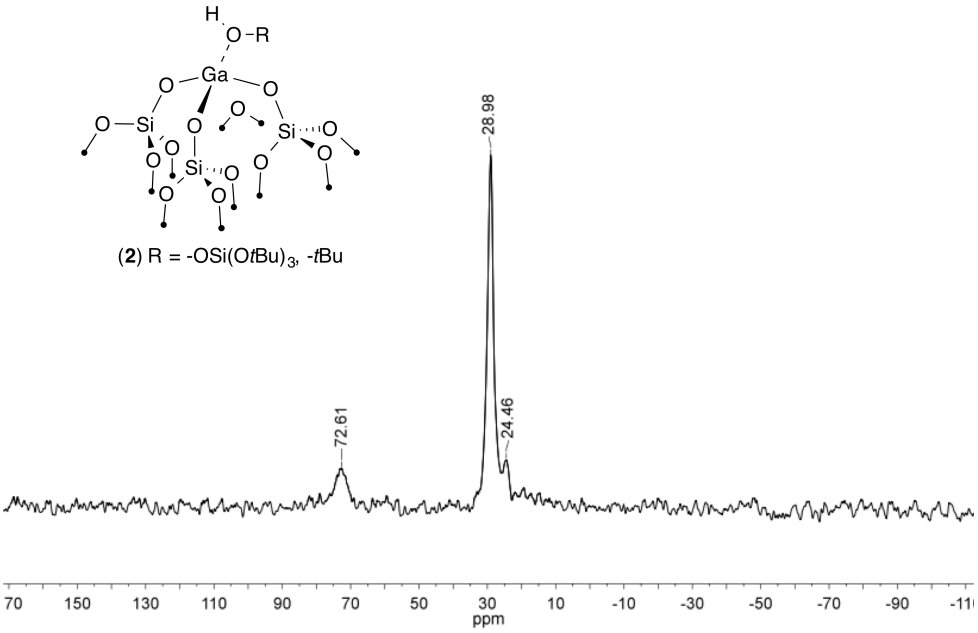

Figure S5. ^{13}C SSNMR of **2** (spinning rate, 10 kHz; scans, 4096; contact time, 3 ms; line broadening, 50 Hz).

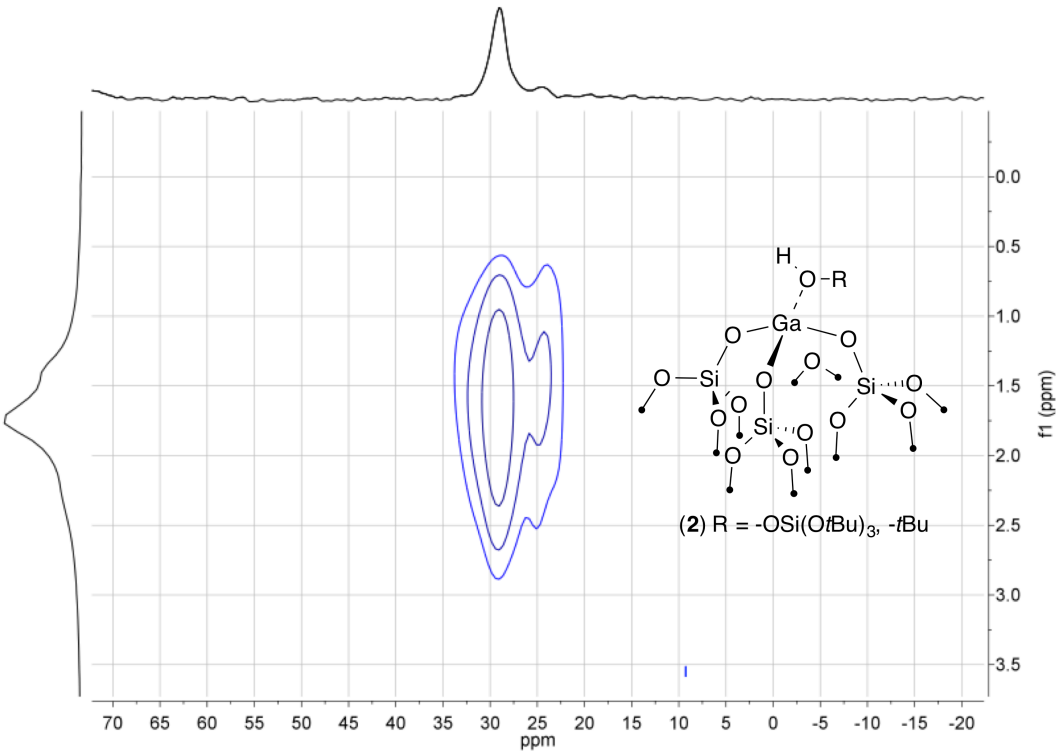

Figure S6. HETCOR SSNMR of **2** (spinning rate, 10 kHz).

Synthesis of [(≡SiO)$_3$Ga(XOSi≡)] (X= H or ≡Si) (3).

To a glass reactor was added **2** (0.825 g, 0.172 mmol Ga). The reactor was subsequently placed under high vacuum (10^{-5} mbar) at heated to 150 °C (5 °C/min) for 2 hours, 300 °C (5 °C/min) for 2 hours, 400 °C (5 °C/min) for 2 hours, and 500 °C (5 °C/min) for 10 hours. Using ^{1}H NMR spectroscopy (300 MHz, 25 °C, d1 = 60 sec) with ferrocene as an internal standard the volatiles liberated from the thermal transformation were quantified revealing isobutene (0.426 mmol). Elemental analysis: Ga, 1.45; H, 0.06.

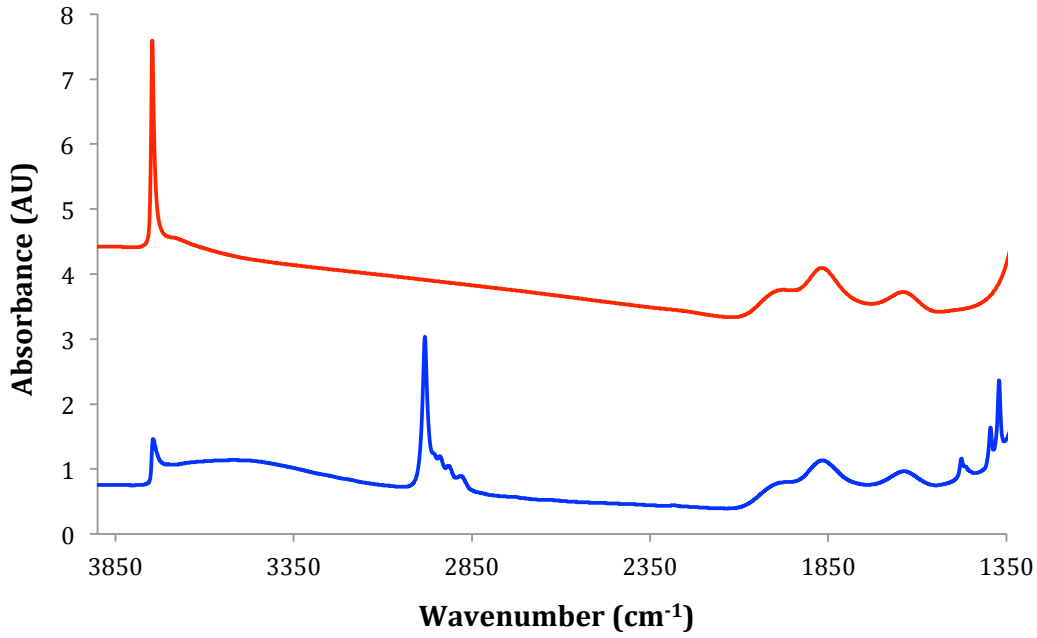

Figure S7. Transmission IR spectra of **3** (top) and **2** (bottom) normalized to the υ_{SiO} vibrational band at 1850 cm^{-1}.

Pyridine adsorption on [(≡SiO)$_3$Ga(XOSi≡)] (X= H or ≡Si) (3).

Pyridine adsorption studies were performed on a pellet of **3** and were monitored by infrared spectroscopy.[3] After exposing **3** to pyridine vapor, the pellet was placed under high vacuum and analyzed at temperature intervals of 100 °C up to 500 °C (5 °C/min). All temperatures and pressures were maintained for a minimum of 15 minutes prior to analysis by infrared spectroscopy. Retention of pyridine up to 500 °C under high vacuum and the presence of only a single set of vibrational bands for a pyridine adduct with relatively narrow full widths at half-maximum indicates the presence of a single type of strong Lewis acid site on the surface.

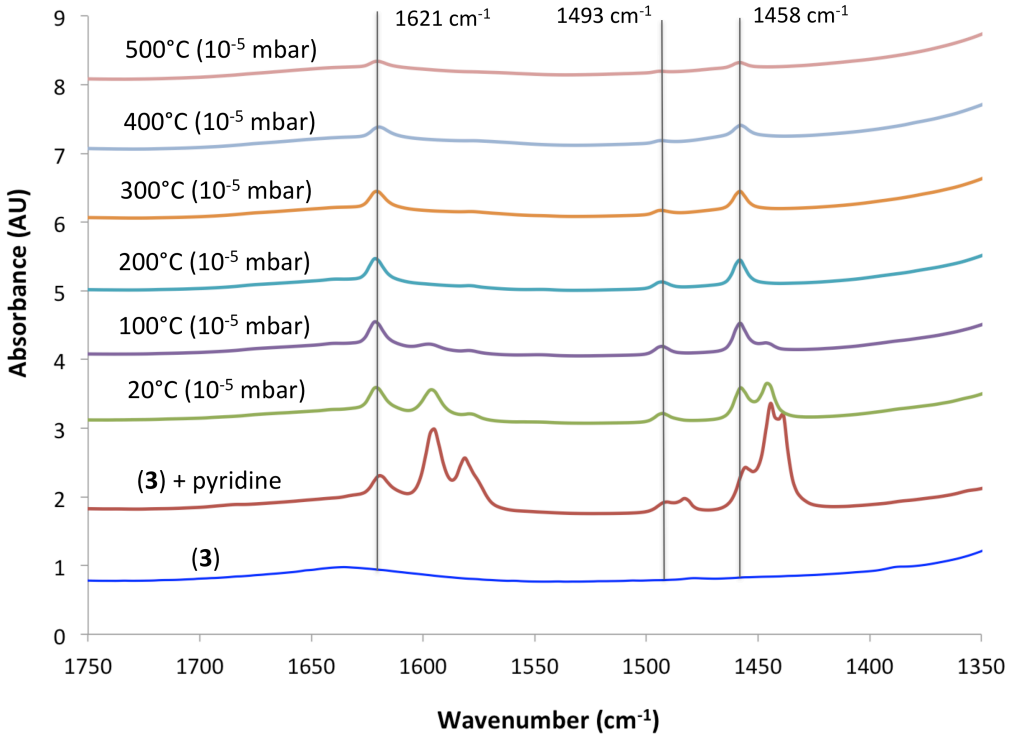

Figure S8. Pyridine adsorption on [(≡SiO)$_3$Ga(XOSi≡)] (X= H or ≡Si) (**3**) followed by treatment at different temperatures under high vacuum.

X-ray Absorption Spectroscopy

Ga K-edge X-ray absorption spectra were measured in transmission mode on the BM01B station of the Swiss Norwegian Beamlines (SNBL) at ESRF, Grenoble, France. The measurements were performed using a Si (111) double crystal monochromator. The second crystal of the monochramator was detuned by 60 % in order to suppress higher harmonic radiation. The intensities of the incident and transmitted X-rays were monitored with ionization chambers (nitrogen and argon gas filled). All spectra were acquired at room temperature in a continuous scanning mode from 10,150 to 11,500 eV, with an energy steps of 0.5 eV for 14 min. The energy was calibrated with a Zn foil (9,659 eV). All samples were measured in the form of pellets prepared and sealed in two aluminized plastic bags (Polyaniline (15 µm), polyethylene (15µm), Al (12µm), polyethylene (75µm) from Gruber-Folien GmbH & Co. KG) using an impulse sealer inside an argon filled glovebox. The outer bag was removed prior to X-ray absorption measurements. X-ray absorption near edge structure (XANES) and the extended X-ray absorption fine structure (EXAFS) were analyzed using the Ifeffit software package.[4] Fits of EXAFS data for complexes **1**–**3** were fitted in *R*-space (1.0-3.5 Å) after a Fourier transform (**1** and **3**, k = 3.0-12.0 $Å^{-1}$; **2**, k = 3.0-11.0 $Å^{-1}$).

Table S1. EXAFS fit parameters for [Ga(OSi(O*t*Bu)$_3$)$_3$(THF)] (**1**), [(≡SiO)$_3$Ga(HOR)], (**2**, R = –Si(O*t*Bu)$_3$ or –*t*Bu), and [(≡SiO)$_3$Ga(XOSi≡)] (**3**, X = H or ≡Si).[a]

Sample	Neighbor	N[b]	r[Å][c]	σ^2[$Å^2$][d]	Eo (eV)	$S0^2$
1	O	3 *	1.788(3)	0.0035(2)	4(1)	1.2
	O	1 *	2.01(1)	0.0035(2)		
	Si	3 *	3.15(2)	0.007(2)		
	O-Si	6 *	3.25(3)	0.007(2)		
	O	3 *	3.50(2)	0.007(2)		
2	O	4.1(4)	1.81(2)	0.008(1)	-1(2)	1.2
	Si	2.0(1.2)	3.17(1)	0.011(6)		
3	O	3.6(5)	1.80(1)	0.008(1)	-1(3)	1.2
	Si	1.4(6)	3.08(3)	0.011 *		

[a] Samples were measured at 295 K in transmission mode. [b] Number of neighbors. [c] Distance between Ga and neighbor. [d] Debye-Waller factor. Set parameters are indicated by (*).

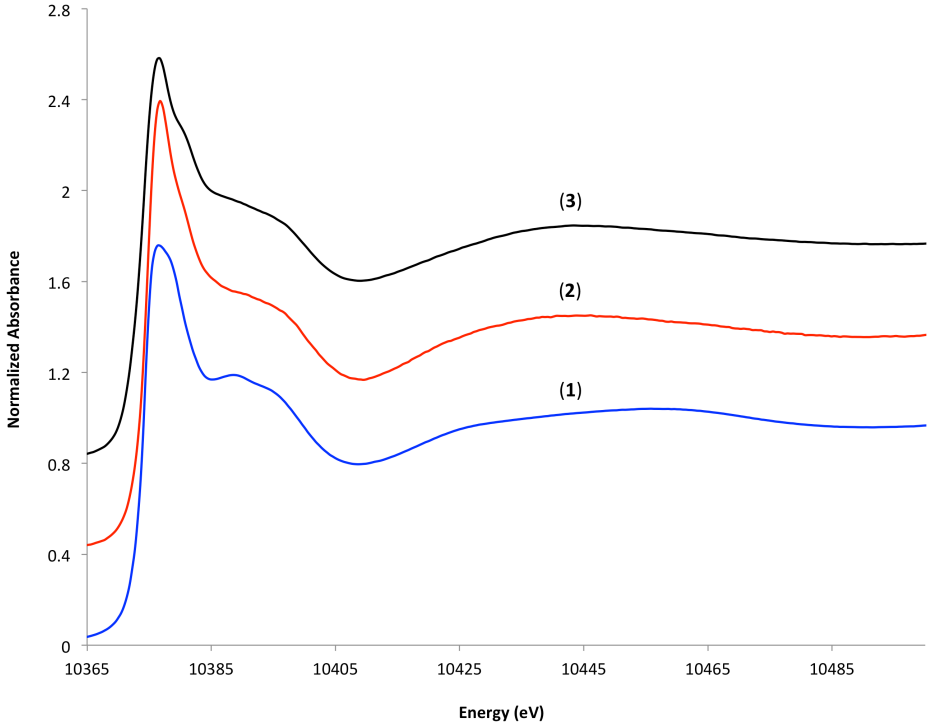

Figure S9. XANES spectra of [Ga(OSi(O*t*Bu)$_3$)$_3$(THF)] (**1**), [(≡SiO)$_3$Ga(HOR)], (R = –Si(O*t*Bu)$_3$ or –*t*Bu) (**2**), and [(≡SiO)$_3$Ga(XOSi≡)] (X= H or ≡Si) (**3**).

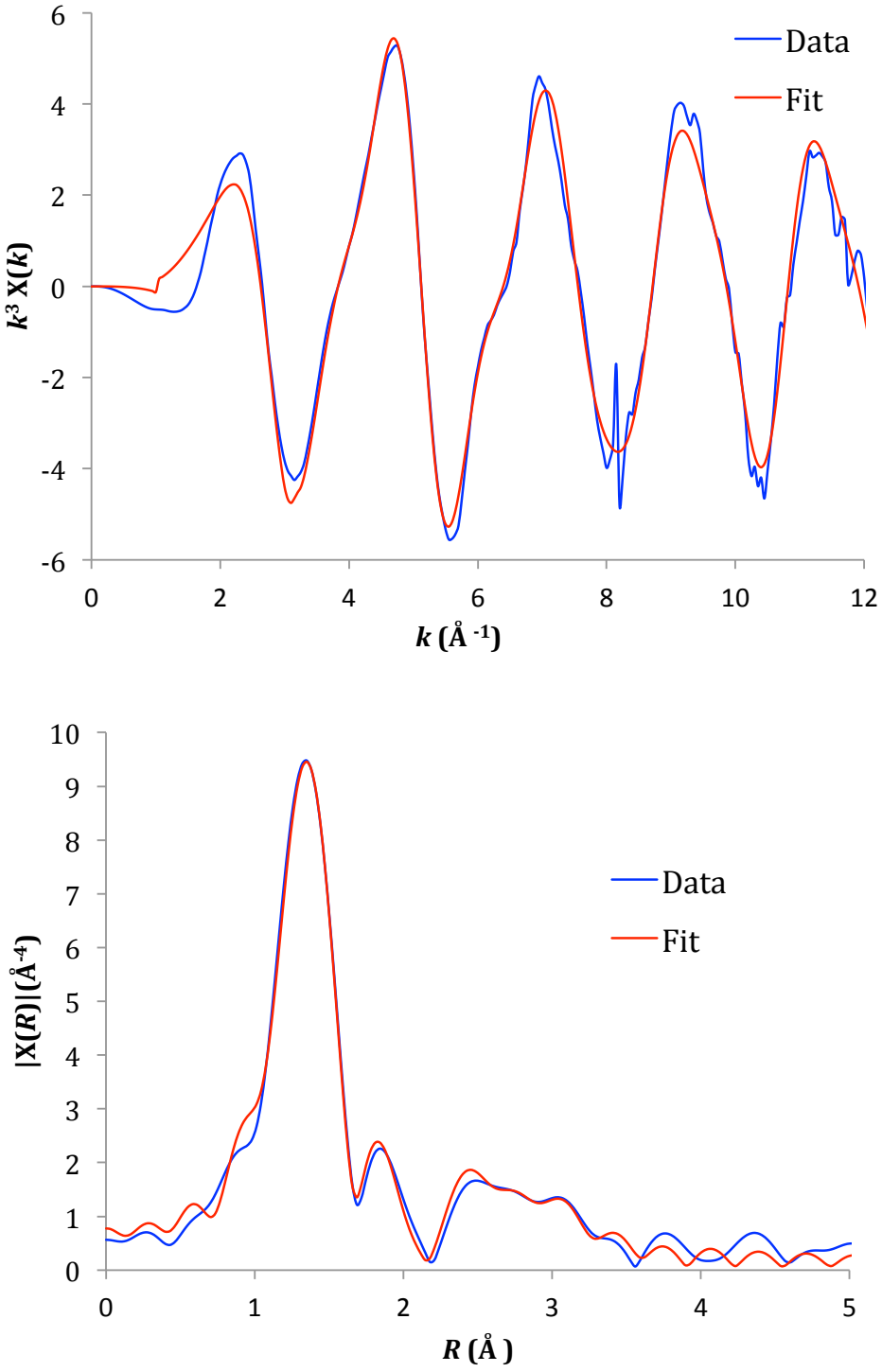

Figure S10. EXAFS data and fit for [Ga(OSi(O*t*Bu)$_3$)$_3$(THF)] (**1**) in *k*-space (top) and *R*-space (bottom).

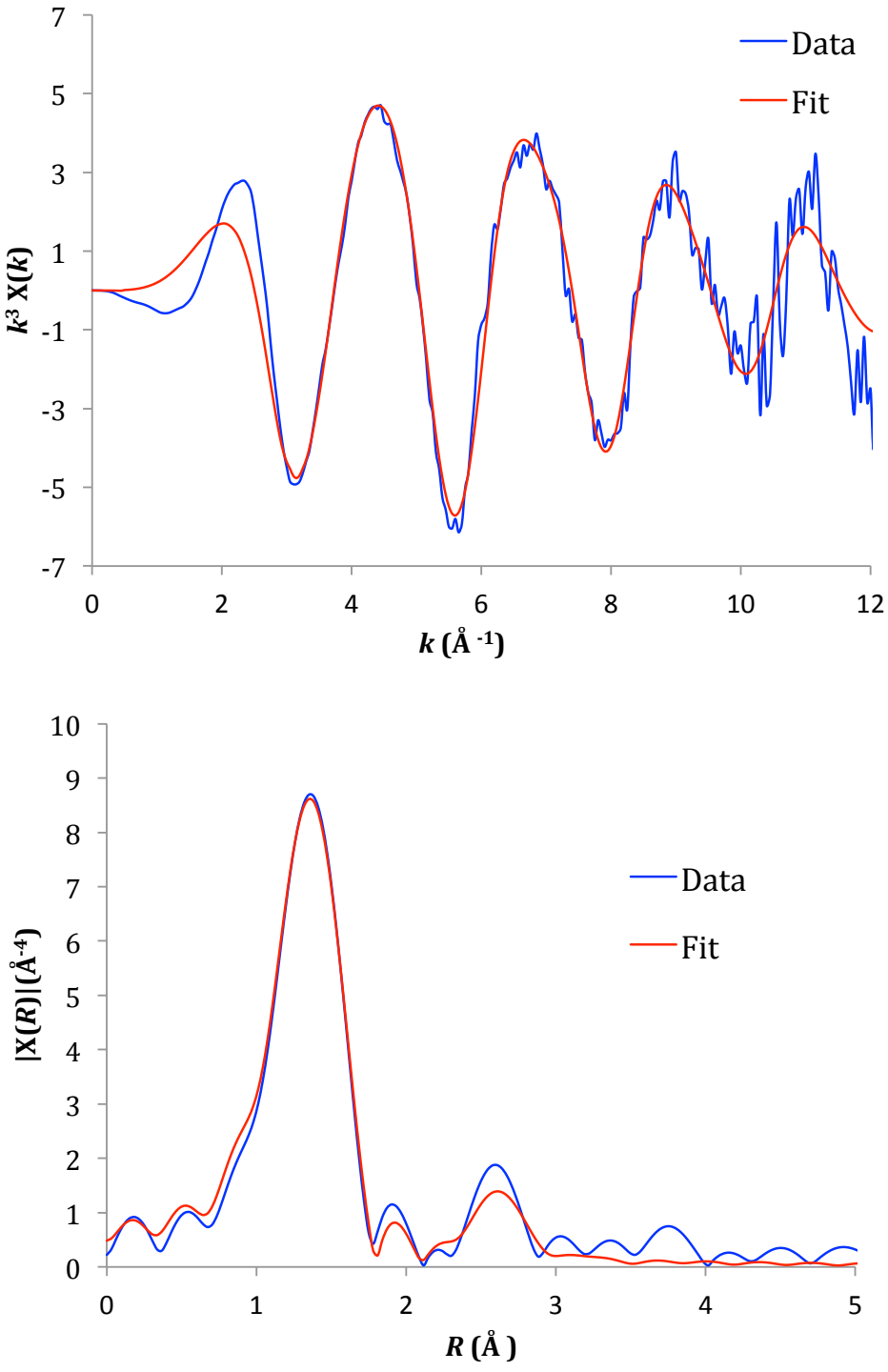

Figure S11. EXAFS data and fit for [(≡SiO)$_3$Ga(HOR)], (R = –Si(O*t*Bu)$_3$ or –*t*Bu) (**2**) in *k*-space (top) and *R*-space (bottom).

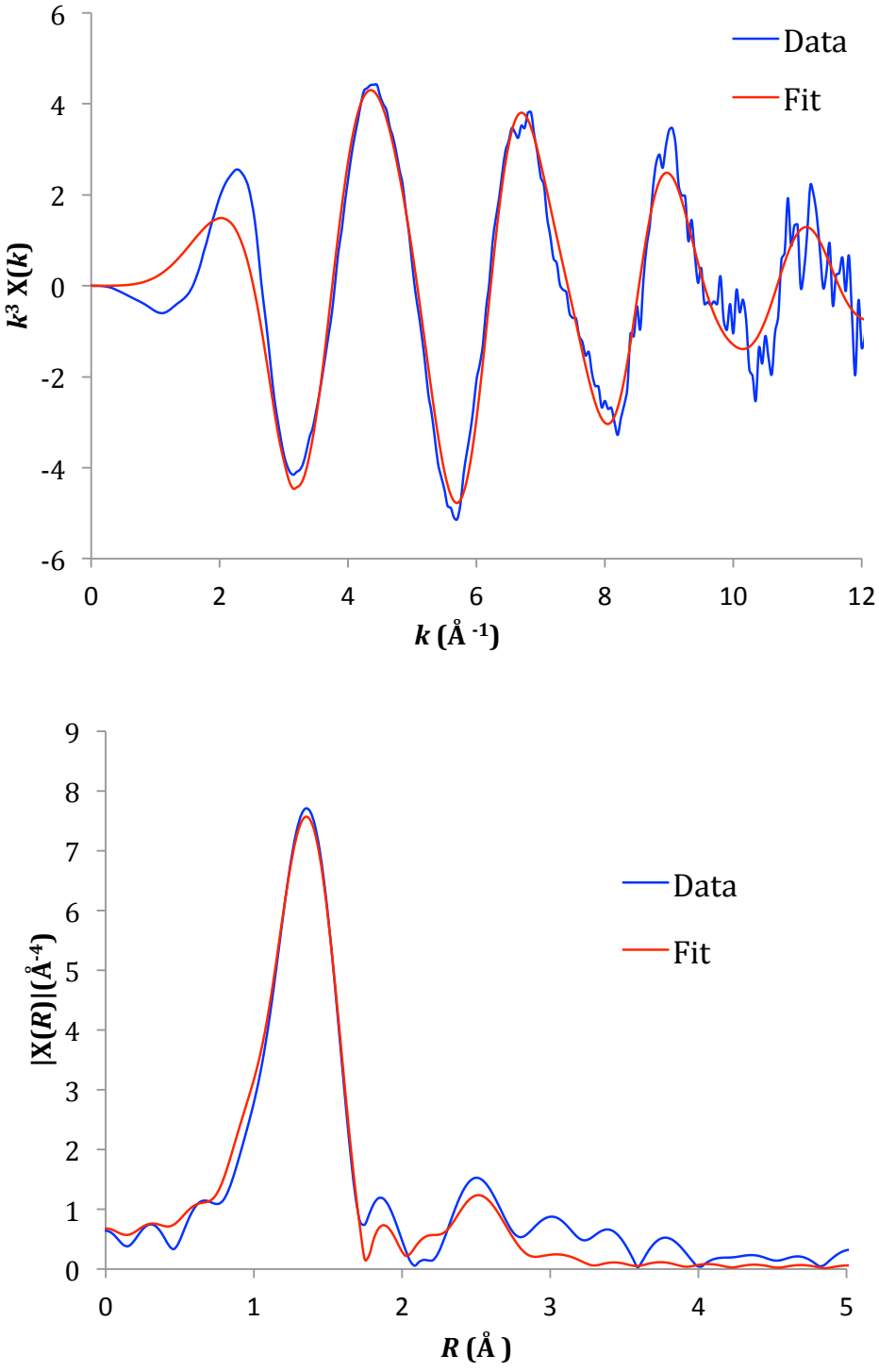

Figure S12. EXAFS data and fit for [(≡SiO)$_3$Ga(XOSi≡)] (X= H or ≡Si) (**3**) in *k*-space (top) and *R*-space (bottom).

Wavelet Transform Analysis

To distinguish between contributions of Ga and Si scatters in the second coordination shell Wavelet transform (WT) analysis of EXAFS spectra was performed.[5] WT consists in replacement of infinitely expanded periodic function in Fourier transformation by a local function, a wavelet. WT allows plotting the experimental EAXFS spectra in two-dimensional form (in *k*- and *R*- space), helping to separate contributions from atoms of different atomic weights. Wavelet transform of a given EXAFS signal $\chi(k)$ is defined as:

$W_f^{\psi}(a,k') = \frac{1}{\sqrt{a}} \int_{-\infty}^{+\infty} \chi(k)\, \psi^* \left(\frac{k-k'}{a}\right) dk$,

where the scalar product of the EXAFS signal and the complex conjugate of the wavelet (ψ^*) is calculated as a function of *a* and *k'*. *a* is the parameter connected with *R* as $a = \frac{\eta}{2R}$ and k' conform to localization of wavelet function in *k* space. In this work was used WT based on Morlet wavelet functions:

$\psi(k) = \frac{1}{\sqrt{2\pi}\sigma} e^{i\eta k} e^{-k^2/2\sigma^2}$,

where parameters σ and η correspond to width and frequency of the wavelet function, respectively. These parameters should be adjusted to get an appropriate resolution in k - an *R*-space. For better quality of WT images we used modified WT functions described elsewhere.[5b] EXAFS data for Ga_2O_3 was obtained from http://ixs.iit.edu/database/data/Farrel_Lytle_data/RAW/Ga/index.html.

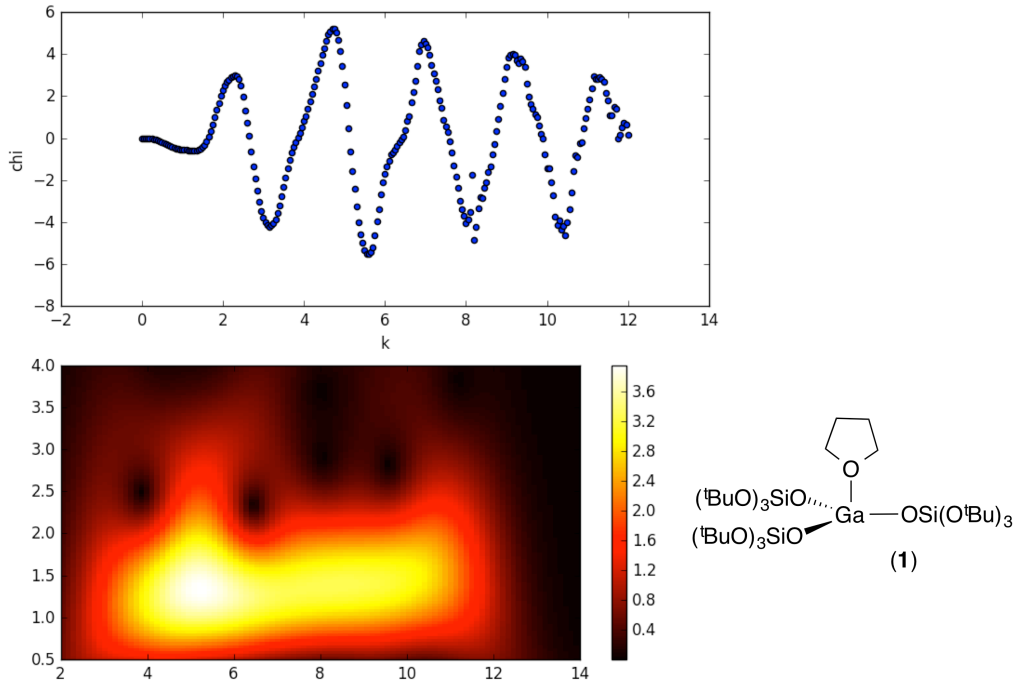

Figure S13. WT analysis of EXAFS data for [Ga(OSi(O*t*Bu)$_3$)$_3$(THF)] (**1**).

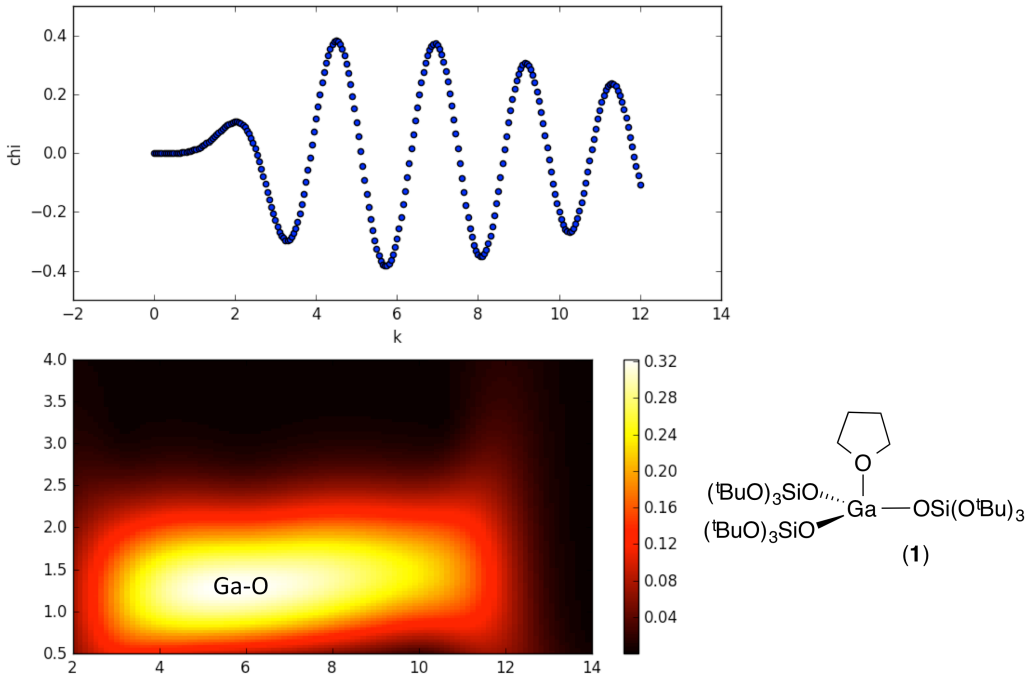

Figure S14. WT analysis of Ga-O scattering path at 1.78 Å for [Ga(OSi(O*t*Bu)$_3$)$_3$(THF)] (**1**).

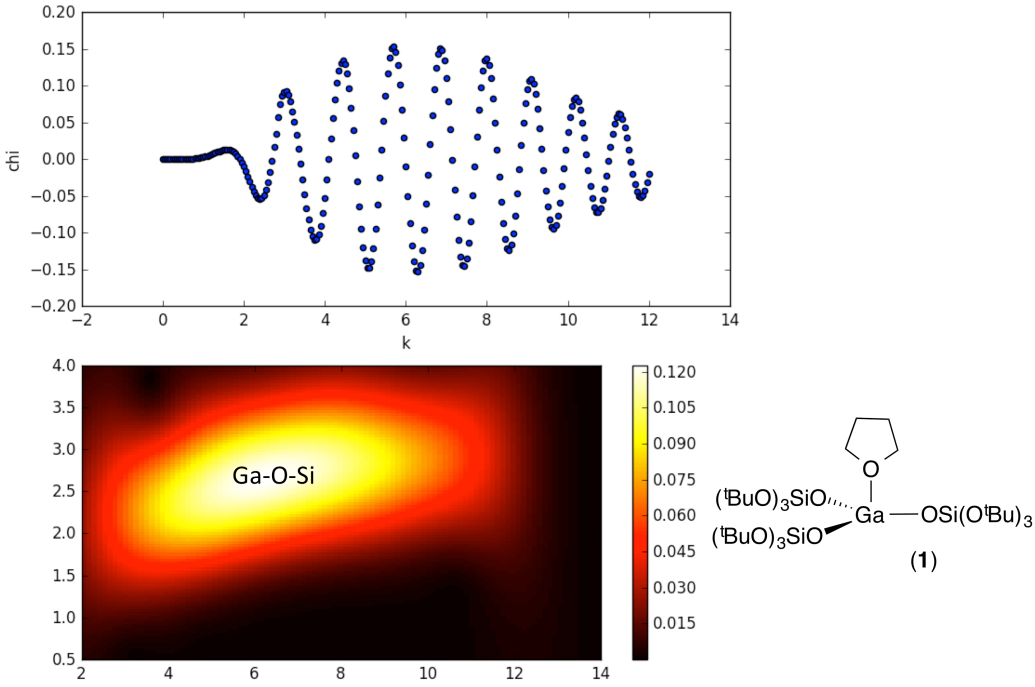

Figure S15. WT analysis of Ga-O-Si scattering path at 3.27 Å for [Ga(OSi(O*t*Bu)$_3$)$_3$(THF)] (**1**).

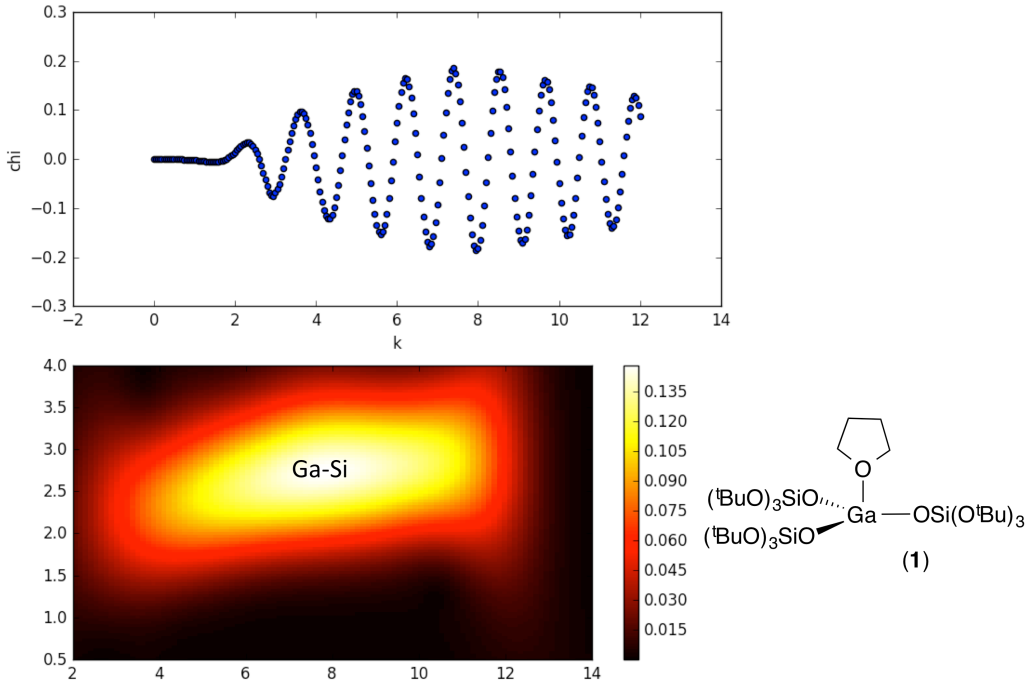

Figure S16. WT analysis of Ga-Si scattering path at 3.17 Å for [Ga(OSi(O*t*Bu)$_3$)$_3$(THF)] (**1**).

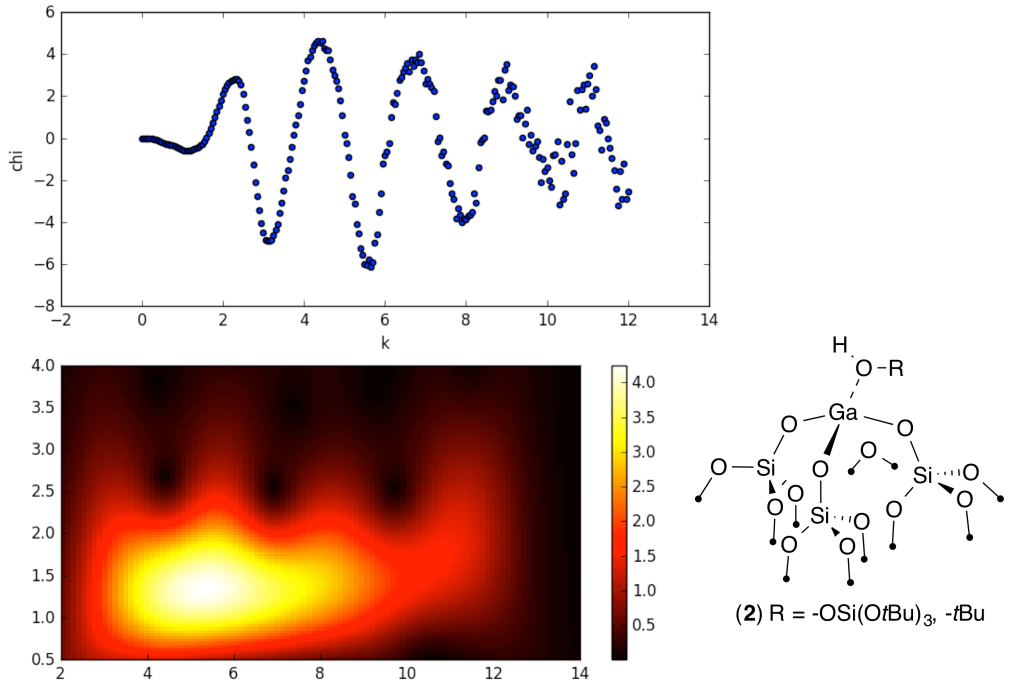

Figure S17. WT analysis of EXAFS data for [(≡SiO)$_3$Ga(HOR)], (R = –Si(O*t*Bu)$_3$ or –*t*Bu) (**2**).

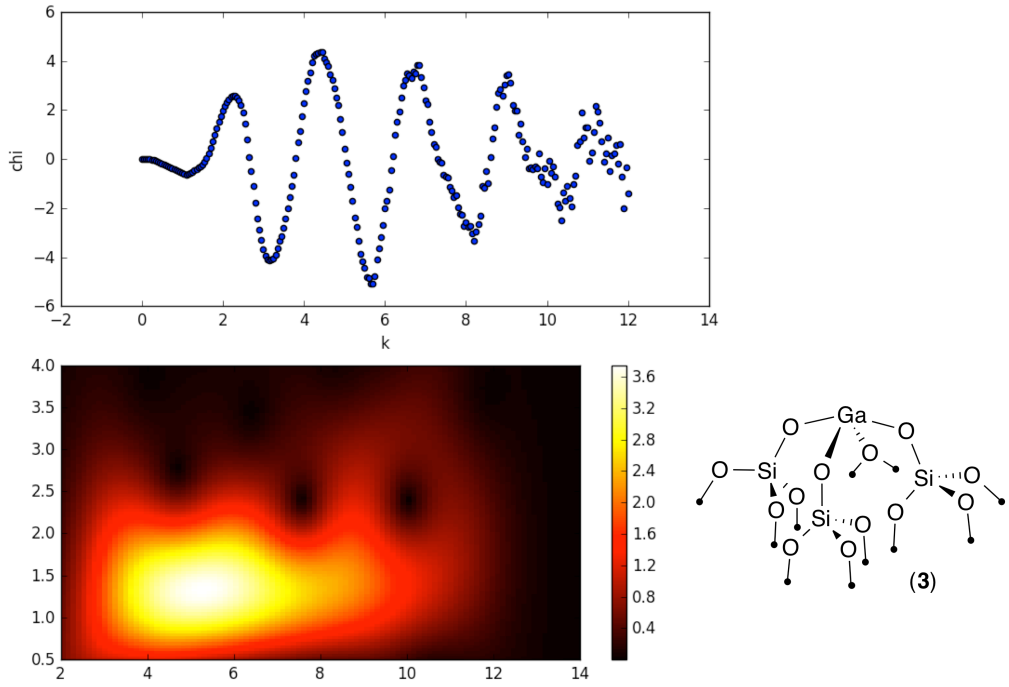

Figure S18. WT analysis of EXAFS data for [(≡SiO)$_3$Ga(XOSi≡)] (X= H or ≡Si) (**3**).

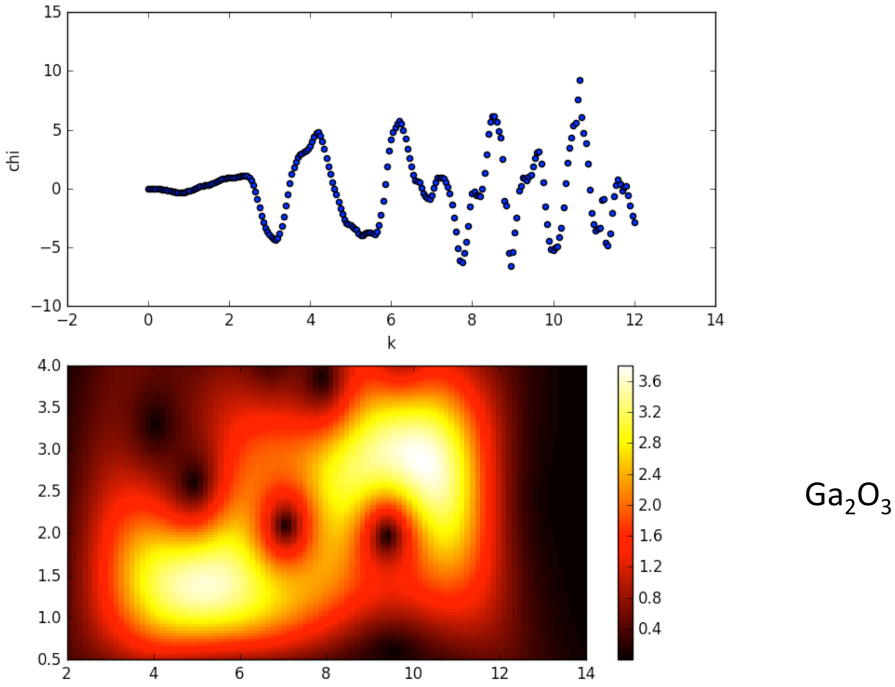

Figure S19. WT analysis of EXAFS data for Ga_2O_3 reference sample.

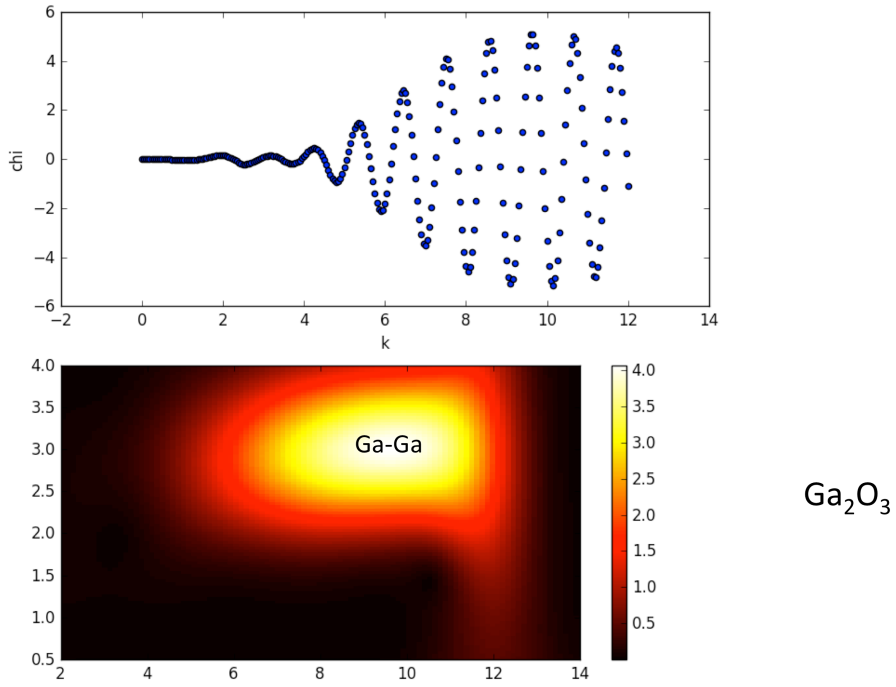

Figure S20. WT analysis of Ga-Ga scattering path at 3.31 Å for Ga_2O_3 reference sample.

Propane Dehydrogenation

Catalytic test were performed utilizing a steel plug-flow reactor designed by PID Engineering. Catalyst samples were loaded into a stainless steel tubular reactor in an Ar filled glovebox. Prior to exposing the catalyst to flow conditions, a bypass was purged for 30 min with Ar (30 mL/min). The samples were then heated to 550 °C utilizing a tubular furnace under a flow of Ar (30 mL/min) and the temperature was maintained for 30 min. The gas mixture was subsequently mixed and purged through a bypass for 20 min prior to contact with the catalyst. Reaction temperatures were maintained utilizing a thermocouple maintained in contact with the catalyst dispersed in SiC to yield a total weight of 2.5 g. The output gas composition was analyzed automatically by a GC injector programmed to sample the gas at specific times throughout the reaction. Gases were purified by passing through a column with molecular sieves and Q5 catalyst prior to introduction to the flow reactor.

The catalytic activity of **3** for propane dehydrogenation was investigated at various flow rates and propane concentrations. Figures S21-S23 show product selectivity, propane conversion, and turnover frequency at a flow of 10 mL/min with 20% C_3H_8/Ar. Figures S24-S26 show product selectivity, propane conversion, and turnover frequency at a flow of 5 mL/min with 20% C_3H_8/Ar. Figures S27-S29 show product selectivity, propane conversion, and turnover frequency at a flow of 20 mL/min with 5% C_3H_8/Ar. Figures S30-S32 show product selectivity, propane conversion, and turnover frequency at a flow of 30 mL/min with 3.3% C_3H_8/Ar. In all cases the white catalyst experienced only minimal darkening over 20 hours of catalytic activity, suggesting that coke formation is a negligible contribution to propane conversion. Propane dehydrogenation was also performed over the surface of $SiO_{2\text{-}700}$ at a flow of 10 mL/min with 20% C_3H_8/Ar yielding a conversion of 1.7% and the following selectivity: C_3H_6, 47.8%; C_2H_4, 25.3%; CH_4, 26.9%.

Table S2. Summary of catalytic propane dehydrogenation at 550 °C utilizing **3**.

Flow Rate	5 mL/min (20% C_3H_8/Ar)	10 mL/min (20% C_3H_8/Ar)	20 mL/min (5.0% C_3H_8/Ar)	30 mL/min (3.3% C_3H_8/Ar)
Ga (mmol)	0.019	0.022	0.016	0.015
Conversion – Initial	9.7 %	9.3 %	4.0 %	4.1 %
TOF (h^{-1}) – Initial	11.8	20.4	5.6	6.0
Selectivity – Initial	C_3H_6 – 92.8 % C_2H_4 – 3.3 % CH_4 – 3.9 %	C_3H_6 – 94.3 % C_2H_4 – 2.6 % CH_4 – 3.1 %	C_3H_6 – 93.5 % C_2H_4 – 3.1 % CH_4 – 3.5 %	C_3H_6 – 91.8 % C_2H_4 – 4.2 % CH_4 – 3.9 %
Conversion – 20 h	5.2%	6.5 %	2.6 %	2.8 %
TOF (h^{-1}) – 20 h	5.9	14.2	3.7	4.1
Selectivity – 20 h	C_3H_6 – 86.8 % C_2H_4 – 5.8 % CH_4 – 7.4 %	C_3H_6 – 93.0 % C_2H_4 – 3.2 % CH_4 – 3.7 %	C_3H_6 – 93.0 % C_2H_4 – 3.4 % CH_4 – 3.6 %	C_3H_6 – 92.0 % C_2H_4 – 4.2 % CH_4 – 3.8 %
k_d (h^{-1})[a]	0.034	0.020	0.023	0.020

[a] $k_d = \ln(1-conv_{end}/conv_{end})-\ln(1-conv_{start}/conv_{start})/t$ ($conv_{start}$, conversion at start of experiment; $conv_{end}$, conversion at end of experiment; t, duration of experiment in hours).[6]

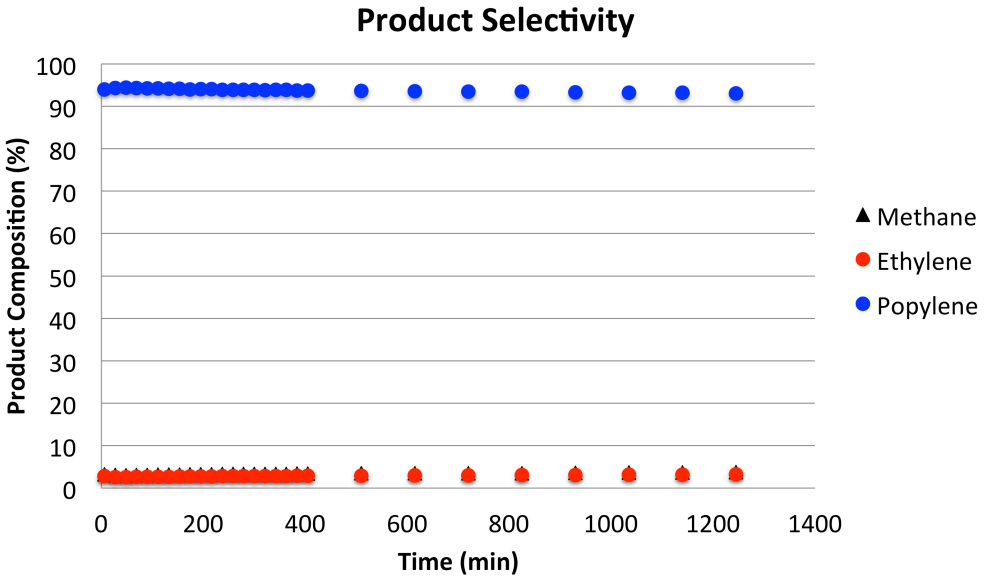

Figure S21. Product selectivity during propane dehydrogenation using **3** monitored over 20 hours at 550 °C with 20 % C_3H_8/Ar at 10 mL/min and a total pressure of 2 bar.

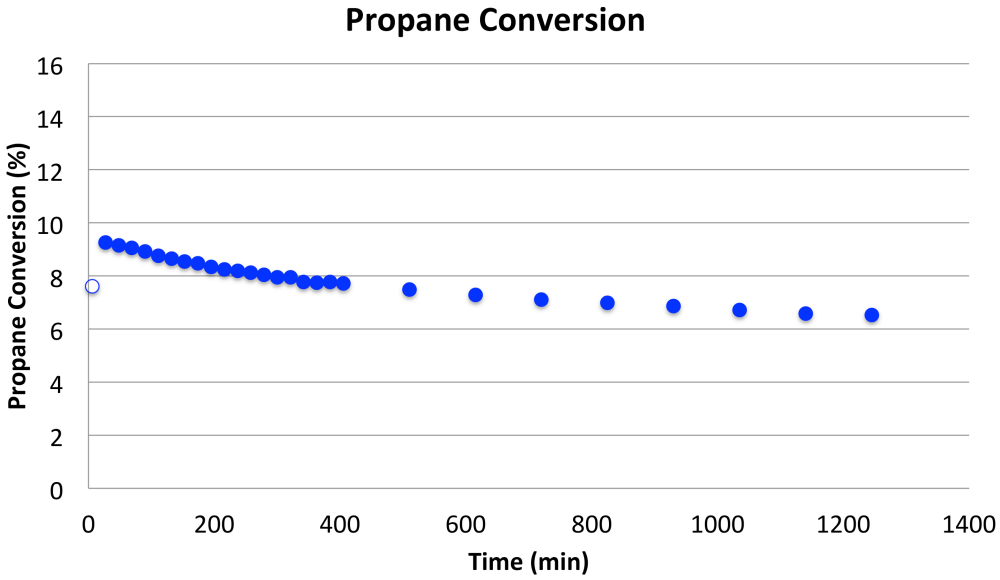

Figure S22. Propane conversion during propane dehydrogenation using **3** monitored over 20 hours at 550 °C with 20 % C_3H_8/Ar at 10 mL/min and a total pressure of 2 bar.

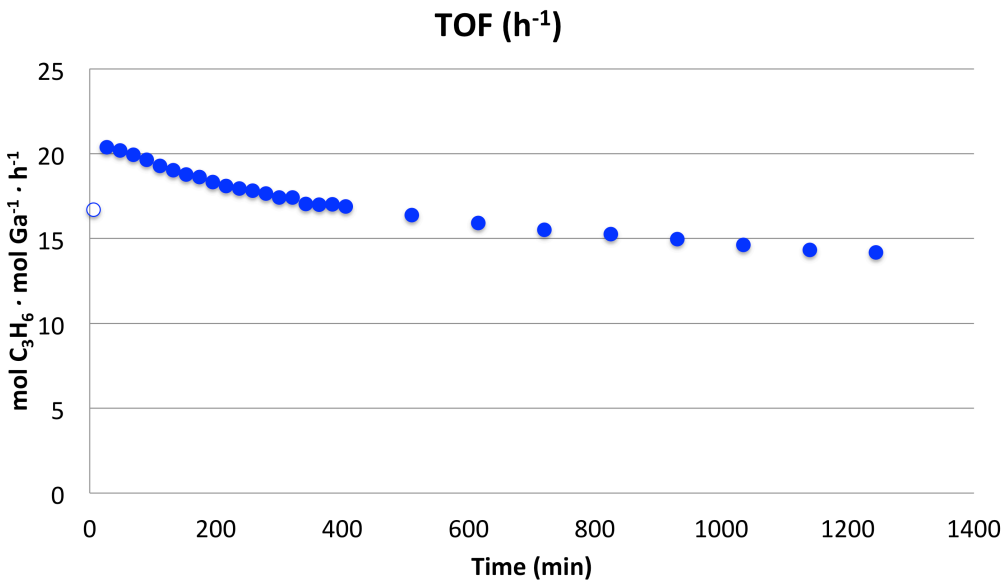

Figure S23. Turnover frequency (h^{-1}) during propane dehydrogenation using **3** monitored over 20 hours at 550 °C with 20 % C_3H_8/Ar at 10 mL/min and a total pressure of 2 bar.

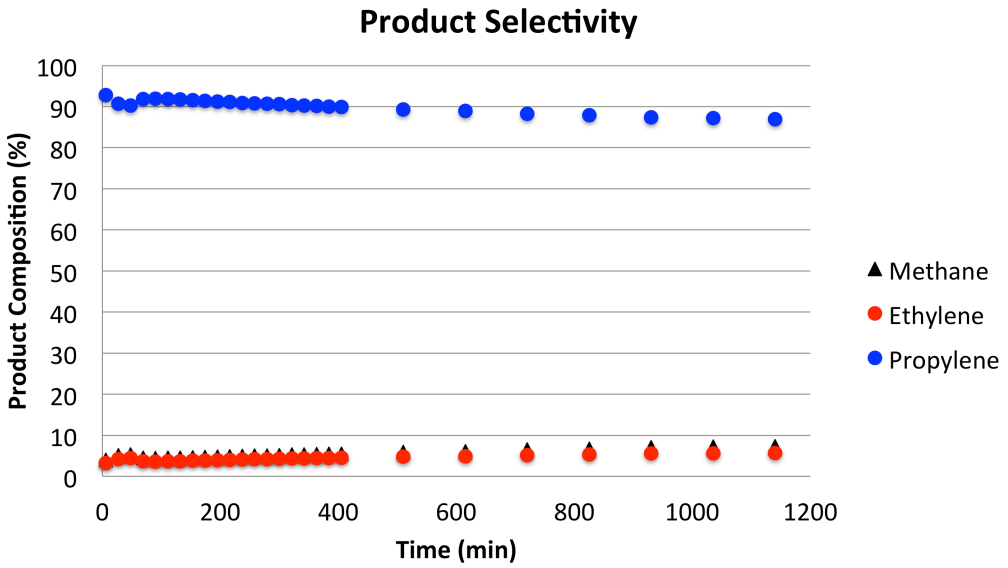

Figure S24. Product selectivity during propane dehydrogenation using **3** monitored over 20 hours at 550 °C with 20 % C_3H_8/Ar at 5 mL/min and a total pressure of 2 bar.

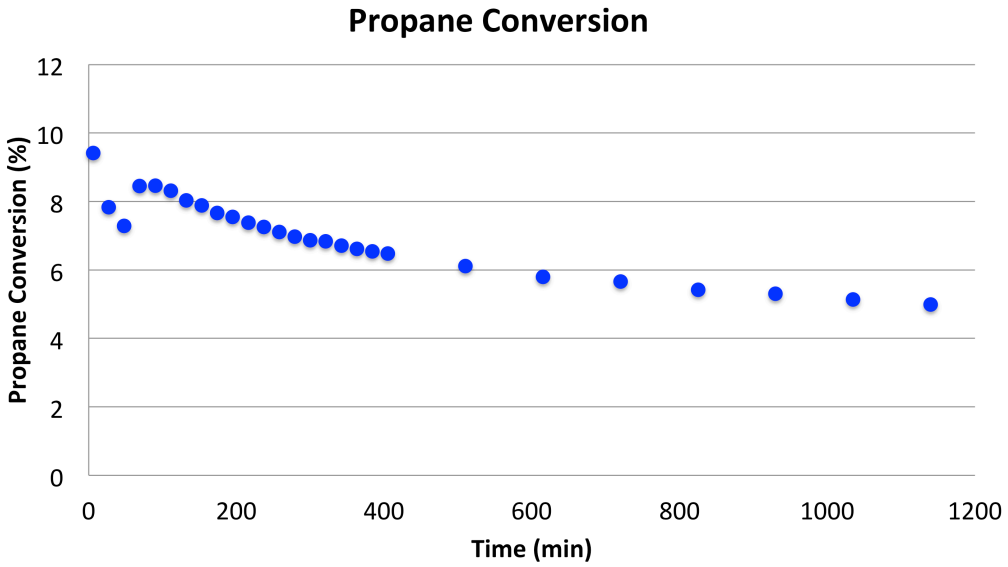

Figure S25. Propane conversion during propane dehydrogenation using **3** monitored over 20 hours at 550 °C with 20 % C_3H_8/Ar at 5 mL/min and a total pressure of 2 bar.

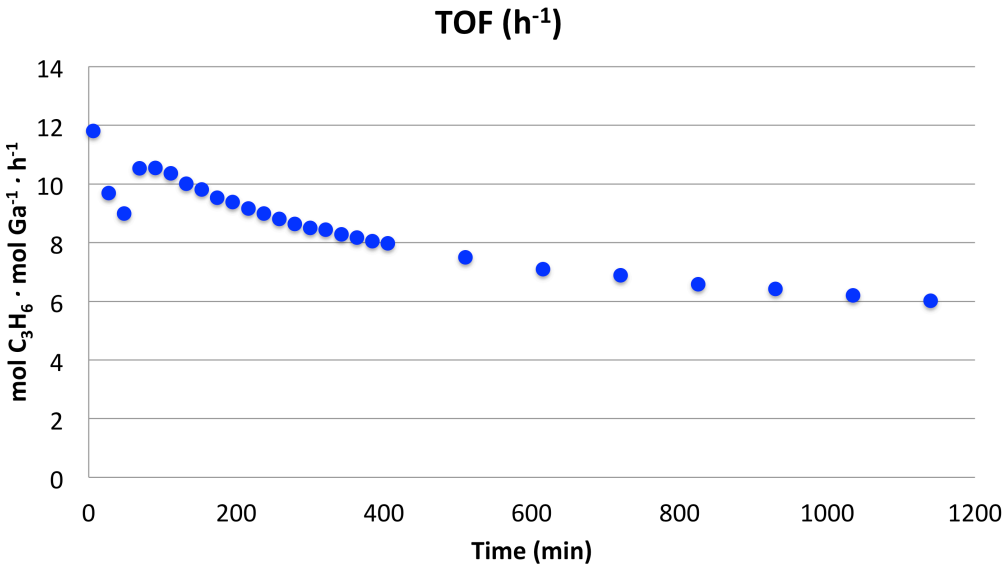

Figure S26. Turnover frequency (h^{-1}) during propane dehydrogenation using **3** monitored over 20 hours at 550 °C with 20 % C_3H_8/Ar at 5 mL/min and a total pressure of 2 bar.

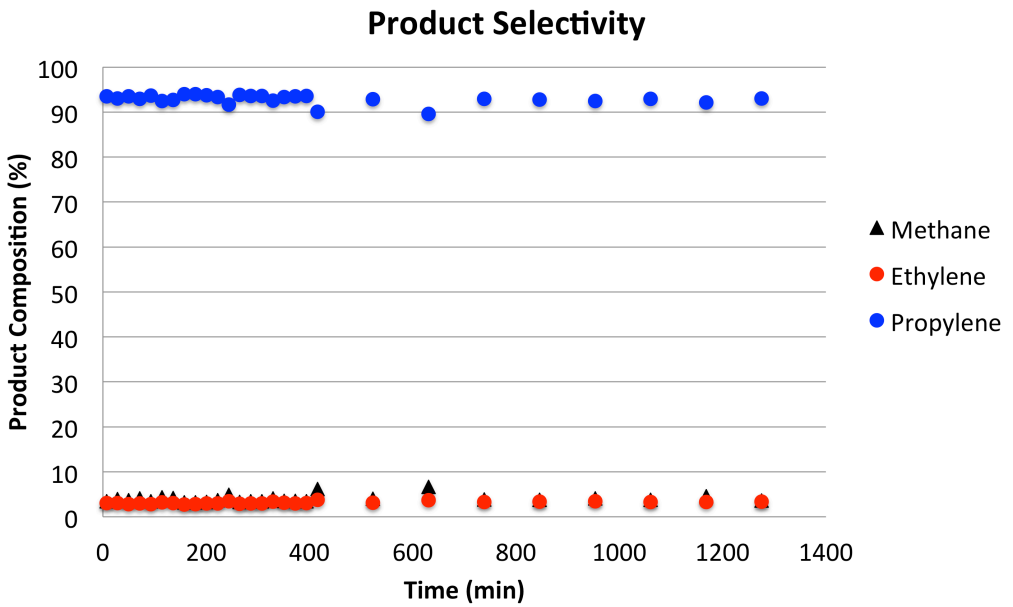

Figure S27. Product selectivity during propane dehydrogenation using **3** monitored over 20 hours at 550 °C with 5 % C_3H_8/Ar at 20 mL/min and a total pressure of 2 bar.

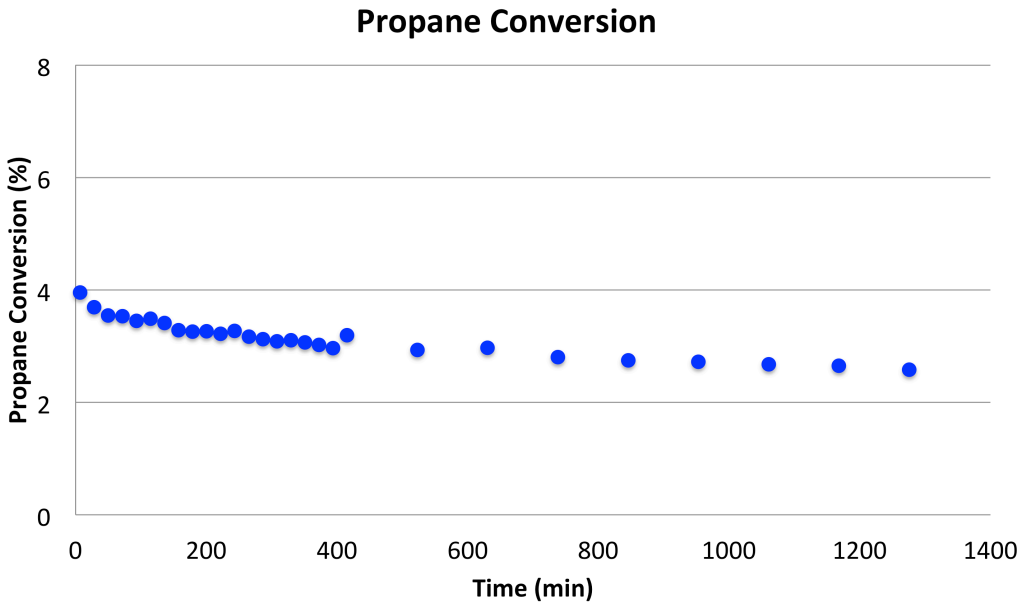

Figure S28. Propane conversion during propane dehydrogenation using **3** monitored over 20 hours at 550 °C with 5 % C_3H_8/Ar at 20 mL/min and a total pressure of 2 bar.

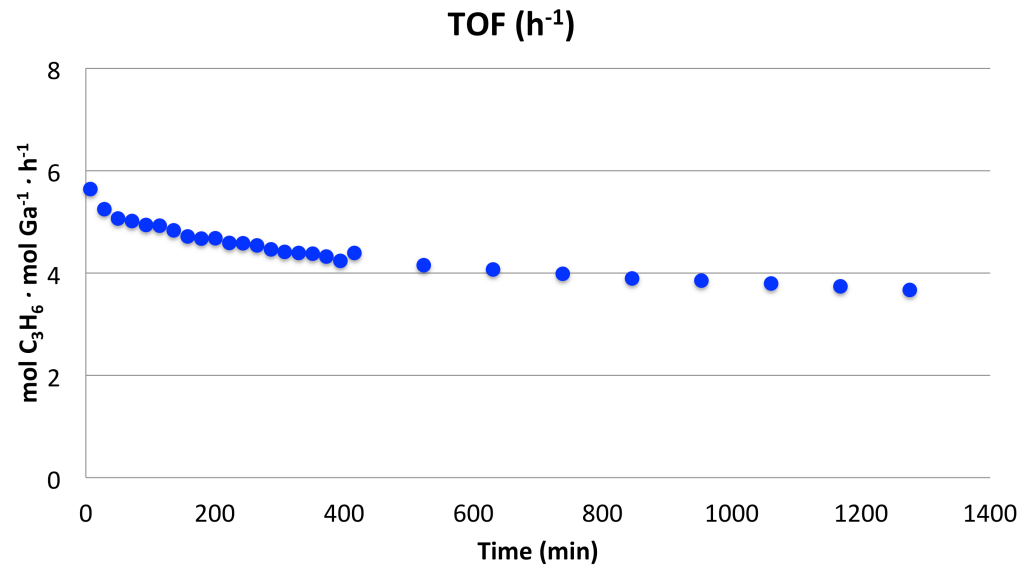

Figure S29. Turnover frequency (h^{-1}) during propane dehydrogenation using **3** monitored over 20 hours at 550 °C with 5 % C_3H_8/Ar at 20 mL/min and a total pressure of 2 bar.

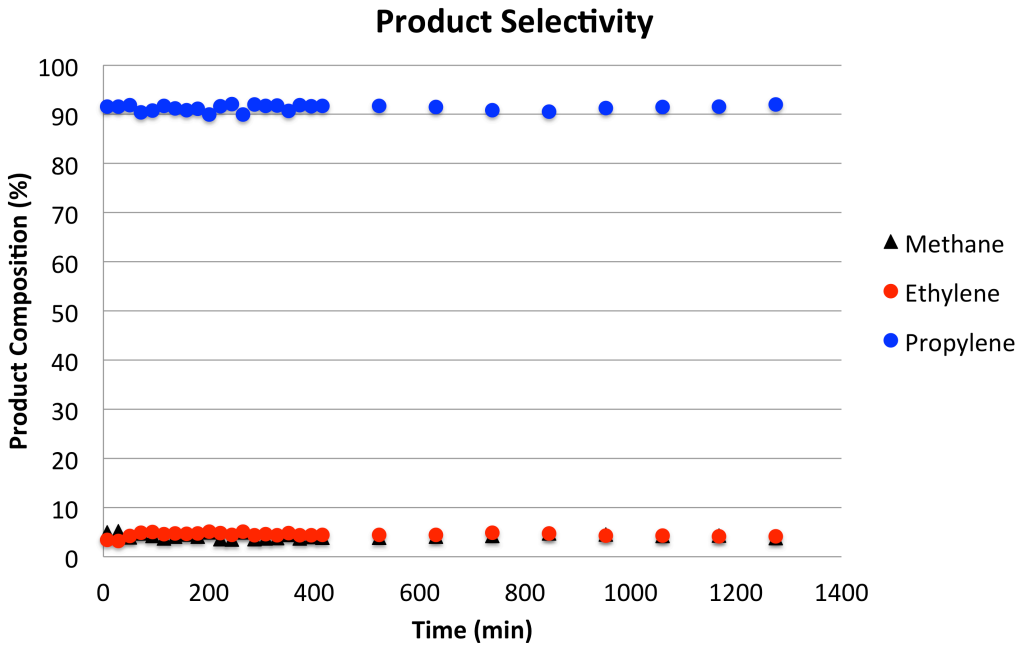

Figure S30. Product selectivity during propane dehydrogenation using **3** monitored over 20 hours at 550 °C with 3.3 % C_3H_8/Ar at 30 mL/min and a total pressure of 2 bar.

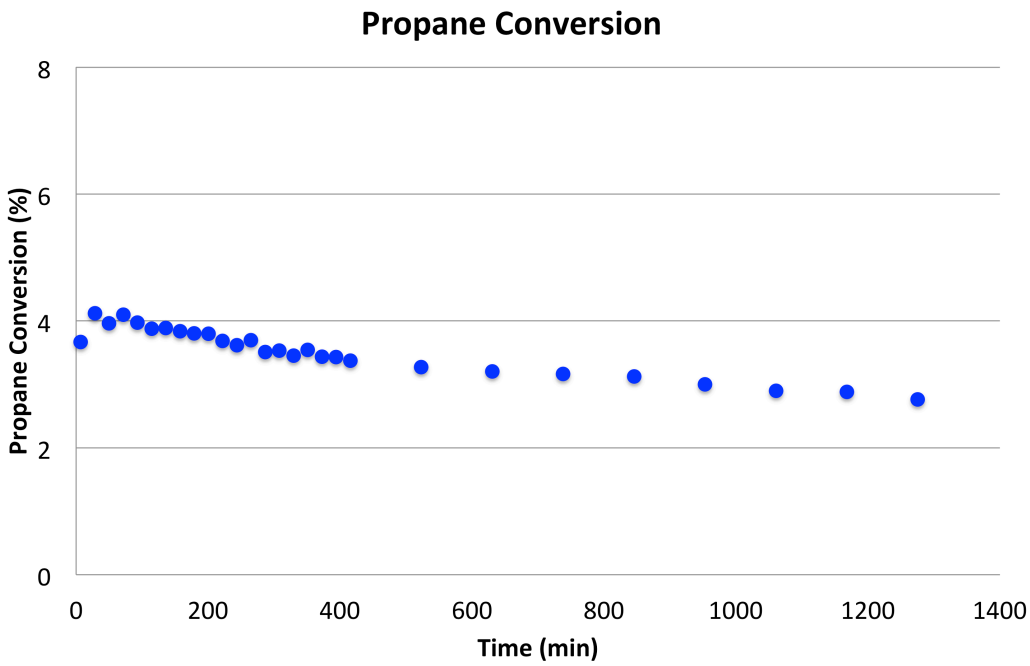

Figure S31. Propane conversion during propane dehydrogenation using **3** monitored over 20 hours at 550 °C with 3.3 % C_3H_8/Ar at 30 mL/min and a total pressure of 2 bar.

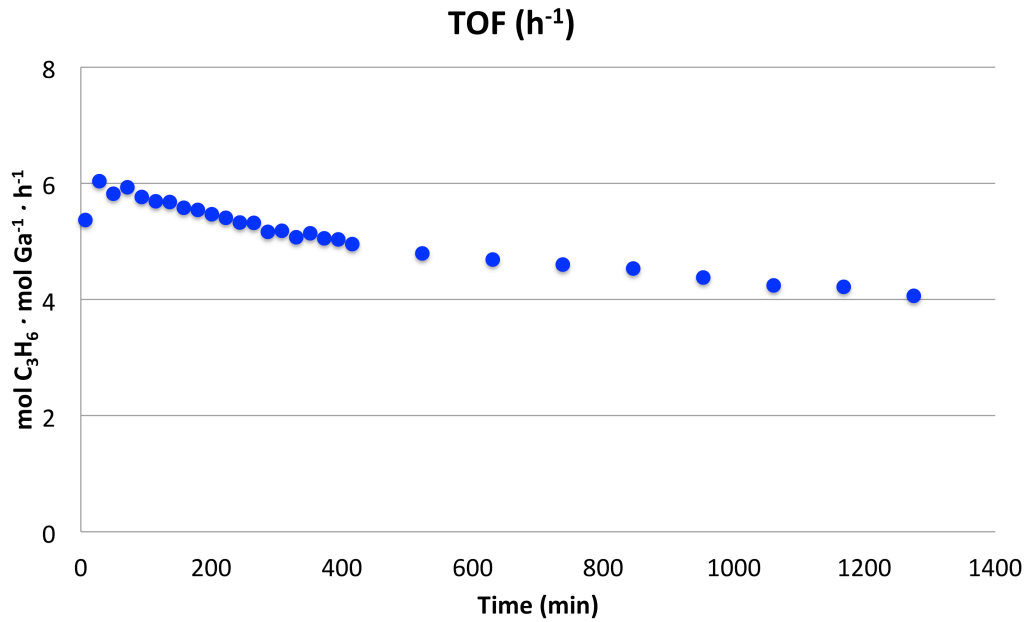

Figure S32. Turnover frequency (h^{-1}) during propane dehydrogenation using **3** monitored over 20 hours at 550 °C with 3.3 % C_3H_8/Ar at 30 mL/min and a total pressure of 2 bar.

Table S3. Comparison of catalytic performances for PDH using **3**, a variety of Ga_2O_3-based catalysts,[6] silica-supported gallium species[3a] and an industrial-like CrO_X-Na/Al_2O_3 catalyst.[6]

Catalyst	Time	Conv.	Sel.	K_d[a]	TOF (h^{-1})[b]	WHSV (h^{-1})
3	Initial	9%	94%	0.022	20.4	2.1
	20 hrs	7%	93%			
Ga_2O_3[c]	Initial	31%	95%	0.67	0.12	1.2
	4 hrs	3%	82%			
β-Ga_2O_3	Initial	33%	95%	0.21	0.0025	0.15
	6 hrs	12%	95%			
Ga_2O_3/SiO_2 (1.7 wt%)	Initial	23%	86%	0.036	1.8	0.97
	6 hrs	20%	80%			
Ga@SiO_2 [d]	--	26%	97%	--	3.8	--
CrO_X-Na/Al_2O_3 (20 wt%)	Initial	47%	80%	0.069	0.027	0.12
	6 hrs	37%	89%			

[a] $k_d = \ln(1-conv_{end}/conv_{end})-\ln(1-conv_{start}/conv_{start})/t$, ($conv_{start}$, conversion at start of experiment; $conv_{end}$, conversion at end of experiment; t, duration of experiment in hours), [b] Highest observed TOF during the reaction,[c] Feed composition of 17% C_3H_8 and 83% CO_2, [d] Catalyst prepared by electrostatic adsorption methods and values obtained at steady state conditions.[3a]

Analysis of [(≡SiO)$_3$Ga(XOSi≡)] (X= H or ≡Si) (3) after catalysis.

XAS measurements were performed on [(≡SiO)$_3$Ga(XOSi≡)] (X= H or ≡Si) (**3**) after catalysis. These results indicate contribution of a new feature with an edge position of 10370.6 eV in the X-ray absorption near-edge structure (XANES) spectrum (Figure S33). This shift in edge energy has previously been attributed to either partial formation of Ga(I) or the presence of Ga(III)–H_X species.[3a] To evaluate this further, infrared analysis of the spent catalyst was also performed (Figure S35). No evidence of vibrational bands characteristic of Ga–H species could be identified in the range of 2100–1900 cm^{-1} in the infrared spectrum. Thus, we attribute this decrease in edge energy to a fraction of Ga(I) species on the surface after catalysis. The extended X-ray absorption fine structure (EXAFS) data obtained after a Fourier transform (k = 3.0-10.0 Å^{-1}) also suggests some structural change of the gallium sites (Figure S34). In comparison to **3**, there is a decrease in intensity of the Ga–O scattering path at ca. 1.4 Å in R-space after PDH. This can be attributed either to the decrease in the number of O neighbors around gallium due to breaking of some Ga–O bonds or to an increase in the static or dynamic disorder for Ga–O bond distances after catalysis. During the partial reduction to Ga(I), additional ≡SiOH are likely generated in close proximity to the reduced gallium sites. This would generate a higher variance in Ga–O bond distances resulting in a decrease in the Ga–O scattering path. Given that migration of Ga sites does not occur (vide infra), we rationalize that the partially reduced gallium sites retain strong interaction with the silica surface, preventing both migration and further reduction. Similar to **3**, EXAFS analysis after catalysis displays no intense feature at higher R-values (2.2-3.5 Å). This indicates that the site-isolation of the Ga sites is retained after PDH.

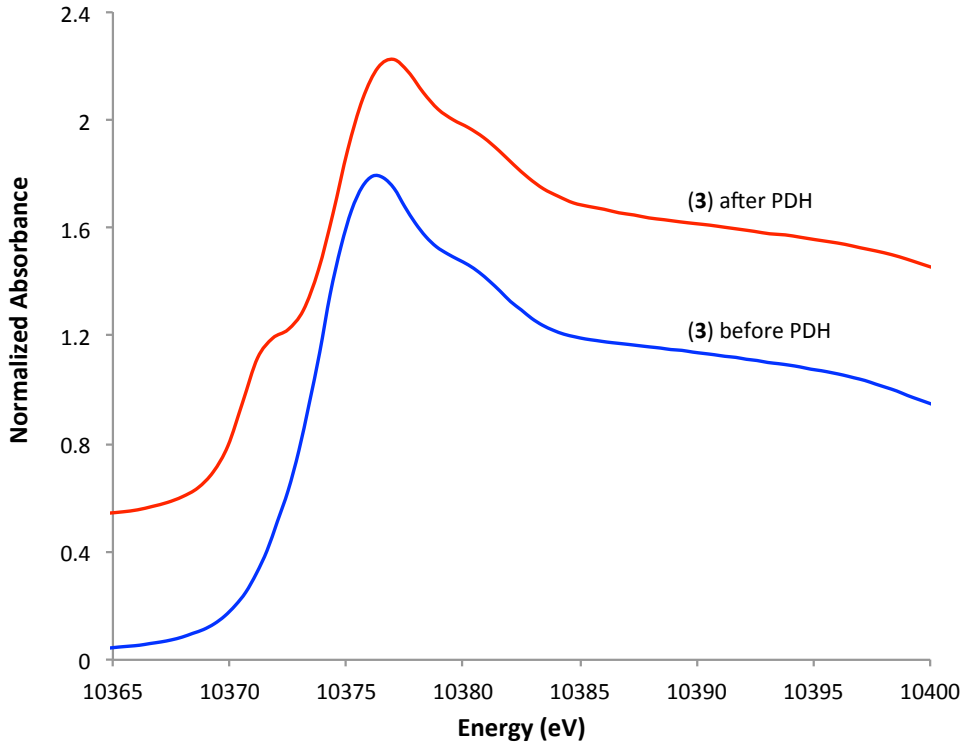

Figure S33. XANES spectra of **3** before (blue) and after (red) PDH. The edge energy after PDH at 10370.6 eV is attributed to partially reduced gallium sites on the surface.

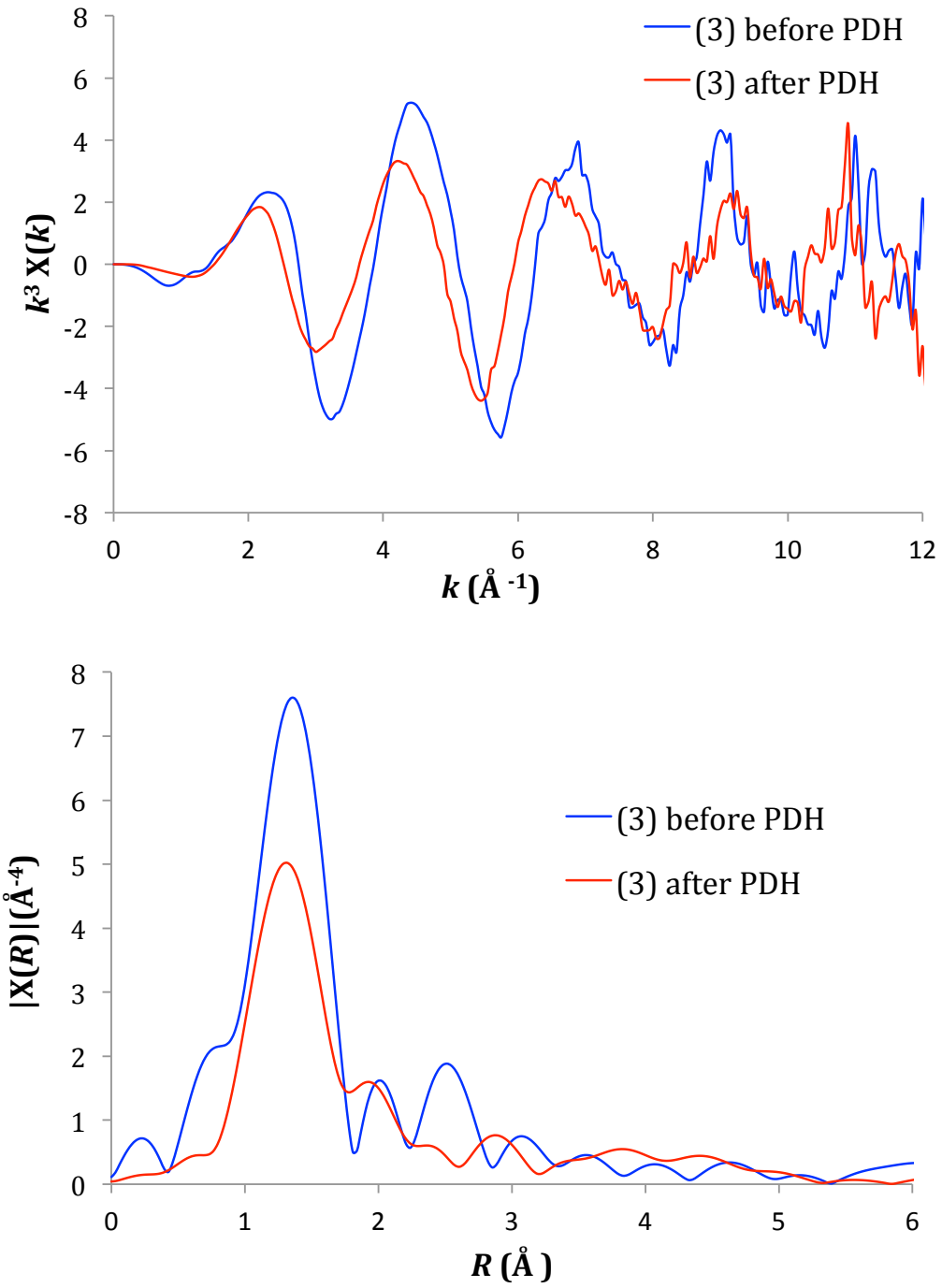

Figure S34. EXAFS data for **3** before and after PDH in *k*-space (top) and *R*-space (bottom).

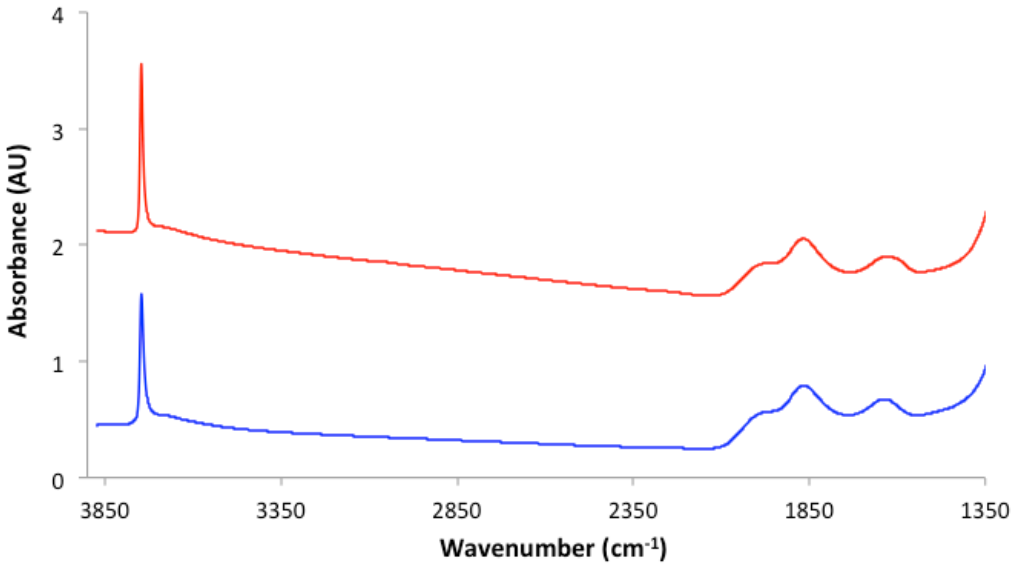

Figure S35. Transmission IR spectra of **3** before (bottom) and after (top) PDH normalized to the υ_{SiO} vibrational band at 1850 cm^{-1}.

Crystallographic Details.

A suitable crystal for analysis of complex **1** (CCDC #1499756) was placed onto the tip of a MiTeGen loop coated in Paratone oil and mounted on an Oxford-Diffraction XCallibur S kappa geometry diffractometer. The data collection was carried out at 100 K using Mo Kα radiation (graphite monochromator). A randomly oriented region of reciprocal space was surveyed to achieve complete data. Sections of frames were collected with 1.0 º steps in ω with 20 s exposure times. The space group was determined based on intensity statistics and systematic absences. Using Olex2[7] the structure was solved with the Superflip package[8] and refined using SHELXL.[9] All non-hydrogen atoms were refined with anisotropic displacement parameters. The hydrogen atoms were placed in ideal positions and refined as riding atoms.

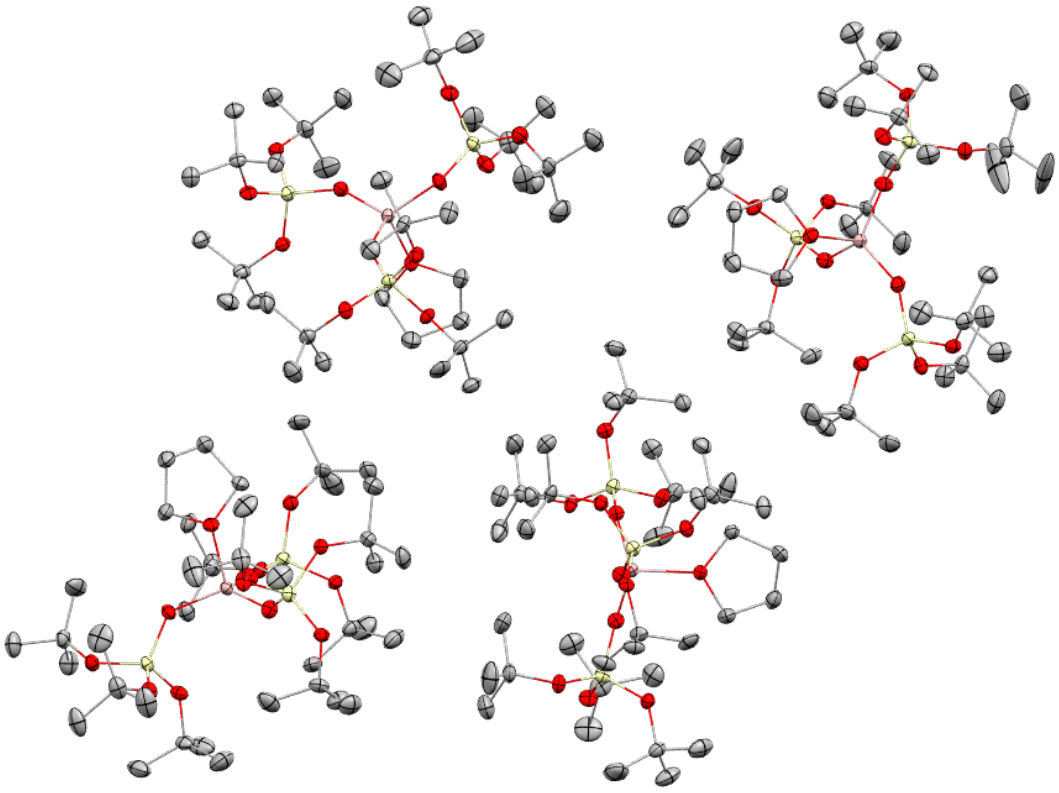

Figure S36. View of the four chemically equivalent molecules that comprise the asymmetric unit of **1**.

Table S4. Crystallographic Parameters for Complex **1**

	1
molecular formula	$C_{40}H_{85}O_{13}Si_3Ga_1$
formula weight	932.10
temp (K)	100
crystal system	Triclinic
space group	*P-1*
cell constants	
a (Å)	18.0886(5)
b (Å)	25.2724(10)
c (Å)	26.1157(10)
α (deg)	62.983(4)
β (deg)	89.953(3)
γ (deg)	89.655(3)
Z	8
V (Å^3)	10635.5(7)
abs coeff (mm^{-1})	0.637
calcd density (g/cm^3)	1.164
F(000)	4048
crystal dimensions (mm)	0.46 x 0.24 x 0.10
wavelength (Å)	0.71073
h,*k*,*l* ranges collected	$-23 \le h \le 24$ $-33 \le k \le 33$ $-34 \le l \le 34$
θ range for data collection (deg)	2.85 to 28.28
number of reflns collected	52326
number of unique reflns	34903
number of parameters	2162
data to parameter ratio	34903/2162
refinement method	Full-matrix least-squares on F^2
R_1[a]	0.0741
wR_2[b]	0.1374
Goodness-of-fit on F^2[c]	1.020

[a] $R_1 = (|F_o| - |F_c|) / |F_o|$. [b] $wR_2 = [[w(F_o^2 - F_c^2)^2] / [w(F_o^2)^2]]^{1/2}$. [c] Goodness-of-fit = $[[w(F_o^2 - F_c^2)^2]/N_{observns} N_{params}]]^{1/2}$, all data

Table S5. Selected Bond Distances for Complex [Ga(OSi(O*t*Bu)$_3$)$_3$(THF)] (**1**), Å

Ga1-O1	1.963(2)	Ga1-O2	1.780(2)	Ga1-O3	1.783(3)
Ga1-O4	1.775(3)				

Table S6. Selected Bond Angles for Complex [Ga(OSi(O*t*Bu)$_3$)$_3$(THF)] (**1**), °

O1-Ga1-O2	104.82(11)	O1-Ga1-O3	97.36(12)	O1-Ga1-O4	101.86(12)
O2-Ga1-O3	119.05(13)	O3-Ga1-O4	115.04(12)	O4-Ga1-O2	114.58(13)

References

[1] A. K. McMullen, T. D. Tilley, A. L. Rheingold, S. J. Geib, *Inorg. Chem.* **1989**, *28*, 3772-3774.

[2] [Ga(OSi(OtBu)$_3$)$_3$(THF)] was disclosed during the course of this study, J. P. Dombrowski, G. R. Johnson, A. T. Bell, T. D. Tilley, *Dalton Trans.* **2016**, *45*, 11025-11034.

[3] a) A. B. Getsoian, U. Das, J. Camacho-Bunquin, G. Zhang, J. R. Gallagher, B. Hu, S. Cheah, J. A. Schaidle, D. A. Ruddy, J. E. Hensley, T. R. Krause, L. A. Curtiss, J. T. Miller, A. S. Hock, *Catal. Sci. Technol.* **2016**, *6*, 6339-6353; b) A. Vimont, J. C. Lavalley, A. Sahibed-Dine, C. Otero Areán, M. Rodríguez Delgado, M. Daturi, *J. Phys. Chem. B* **2005**, *109*, 9656-9664; c) E. P. Parry, *J. Catal.* **1963**, *2*, 371-379.

[4] M. Newville, *J. Synchrotron Radiat.* **2001**, *8*, 322-324.

[5] a) H. Funke, M. Chukalina, A. C. Scheinost, *J. Synchrotron Radiat.* **2007**, *14*, 426-432; b) J. Timoshenko, A. Kuzmin, *Computer Physics Communications* **2009**, *180*, 920-925; c) T. J. Penfold, I. Tavernelli, C. J. Milne, M. Reinhard, A. E. Nahhas, R. Abela, U. Rothlisberger, M. Chergui, *The Journal of Chemical Physics* **2013**, *138*, 014104.

[6] J. J. H. B. Sattler, J. Ruiz-Martinez, E. Santillan-Jimenez, B. M. Weckhuysen, *Chem. Rev.* **2014**, *114*, 10613-10653.

[7] O. V. Dolomanov, L. J. Bourhis, R. J. Gildea, J. A. K. Howard, H. Puschmann, *Journal of Applied Crystallography* **2009**, *42*, 339-341.

[8] a) L. Palatinus, S. J. Prathapa, S. van Smaalen, *Journal of Applied Crystallography* **2012**, *45*, 575-580; b) L. Palatinus, A. van der Lee, *Journal of Applied Crystallography* **2008**, *41*, 975-984; c) L. Palatinus, G. Chapuis, *Journal of Applied Crystallography* **2007**, *40*, 786-790.

[9] G. Sheldrick, *Acta Crystallographica Section C* **2015**, *71*, 3-8.